UiT The Arctic University of Norway

Faculty of Engineering Science and Technology

Department of Computer Science and Computational Engineering

Master of Science Engineering Design

Design and Optimization of Conveyor Belt Rollers

Ahmad Kamel Fadel

Master’s thesis in Engineering Design May-2024

Table of Content

List of Figures

List of Tables

Abstract

Belt conveyor systems play a crucial role in the continuous transportation of bulk materials across varying distances. However, ensuring the reliability of these systems remains a significant concern for operators due to the potential financial losses incurred from system downtime, which not only impacts revenue from material conveying but also disrupts subsequent material processing facilities. The reliability of a belt conveyor system is contingent upon its main components, including the belt, pulleys, drive unit, and idler rolls.

This master's thesis addresses the persistent replacement challenges of conveyor rollers at LKAB's Narvik facility, crucial for the iron ore transportation system. Through a comprehensive approach integrating engineering solutions, operational considerations, and user-oriented factors, the thesis aims to extend roller lifespan while optimizing the roller structure within practical constraints. Emphasizing elevating performance, lifespan, and serviceability, the project is divided into two main sections structural study of the idler set, and investigates existing challenges and identifies factors contributing to frequent replacements, laying the groundwork for developing effective solutions.

Furthermore, in the process of considering parameters like regulatory compliance, load specifications, temperature constraints, and environmental factors, the main focus is to enhance the design of the roller idler. This optimization involves considerations such as weight optimization, ease of maintenance, and environmental compatibility. Through analytical calculations, FEM static and modal analysis, and material selection, HDPE material was proposed the structural behaviour of the roller was studied. Around 30% mass reduction was achieved between the existing and the proposed models. Moreover, other aspects of idlers was studied, including bearing lifespan, and factors that affect their performance, where a solution of shielded bearing was proposed as a solution to prevent the accumulation of contaminants on bearing race.

Further work chapter, outlined aspects requiring further investigation, particularly elaborating on the introduction of an alternative solution to address both vibration and contamination concerns.

Chapter 1: Introduction

1.1 Background and Context

The aim of this chapter is to describe the project background, introduce the industry from where the topic has been originated, and highlight the project objectives. This brief but comprehensive introduction will not only provide the reader with the basic information that applies to this paper but also provide a basic framework for the paper.

Bulk material handling is the engineering field that predominantly deals with moving large amounts of dry material from one location to another, often from the mine site to a processing plant or from a processing facility to a transport mode such as ships or trains. Today's practises can be traced back through history. An early example of bulk material handling is a shaduf, used by ancient Egyptians to irrigate cultivations with water from the Nile River [1] explains that early modern bulk material handling started in the late 1700s, where human powered bucket conveyors or lifts we use to stack ships with primary produce. In 1804 the first steam powered conveyor was commissioned in a bakery as a time saving device, using cloth and leather as belting material [2]. The first mining conveyor was invented in 1905 by Irish-born engineer and inventor, Richard Sutcliffe [2]**.** It was also the world's first underground conveyor and the conveyor belt revolutionised the mining industry forever. The belt was made with cotton and rubber panels. Bulk material handling became very popular during World War II with the development of synthetic materials for belting [3]. Mainly due to the scarcity of natural materials such as cotton. Today, bulk material handling systems incorporate a variety of machines such as screw conveyors or augers, stackers, reclaims, rail cars, bucket elevators and the most common, troughed belt conveyors [3]**.**

1.2 Luossavaara-Kiirunavaara Aktiebolag (LKAB)

An important contributor in Sweden economy is the processing of natural resources, making Sweden one of the EU leading mining nation as it accounts 91% of the iron ore, as well as 9% of the copper, and 24-39% of its lead, zinc, silver, and gold resources [4]. Moreover, iron ore transportation forms around 49% of Sweden's cargo transports, and 60% of Norway's ones [5]. Which in results makes Luossavaara-Kiirunavaara Aktiebolag (LKAB) one of the biggest iron ore producer in Europe. Most of LKAB ore deposits are extracted from underground mines but some of them are also from the open pit. As shown in Figure 1–1, iron ore is mined at Kiruna, Malmberget, Svappavaara in northern Sweden and transported via LKAB transportation system

train railway to Lulea's, and Narvik's ports to be shipped out to the rest of the world. The final product goes through a procedure to reach Narvik, starting from mining phase, were ore is processed to increase the quality of the final product. Iron ore goes through different stages staring from separation of wastes from the ore body, going to the other stage which is concentration, and finally pelletzation stage where the ore is transformed into pellet shape making it easier to transport. Knowing that all the above stages are not done in any of the transporting facilities [4]. However, all previous stages are done in mining cites before being transported to shipping ports.

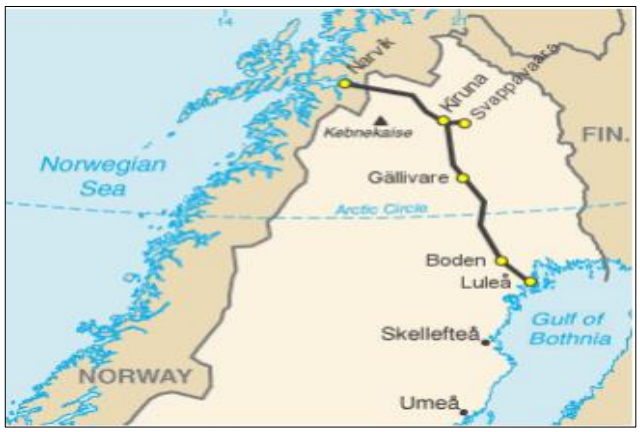

Figure 1–1: Map showing Ore trains Malmbanan connections to Narvik / Luleå ports [6]

1.3 Luossavaara-Kiirunavaara Aktiebolag (LKAB) harbour Narvik

Narvik is considered to be LKAB's gate to the world since its harbor is ice free all over the year.One of the main system that are found in Narvik's harbor is the iron ore storage system 'SILA'. With a total of 2.8 kilometers of tunnels that have been driven under the silos, SILA consist of 12 silos, the silos have a depth of 60 meters and a diameter of 38 meters with a storage capacity of 1.5Mt, and 30Mt annually [5]. Narvik's port receive 68 train wagons per day divided on 10 trains, with a total capacity of 90000 tons. Storage procedure is done by a conveying system shown in Figure 1–2, which is designed to convey material in a continuous manner.

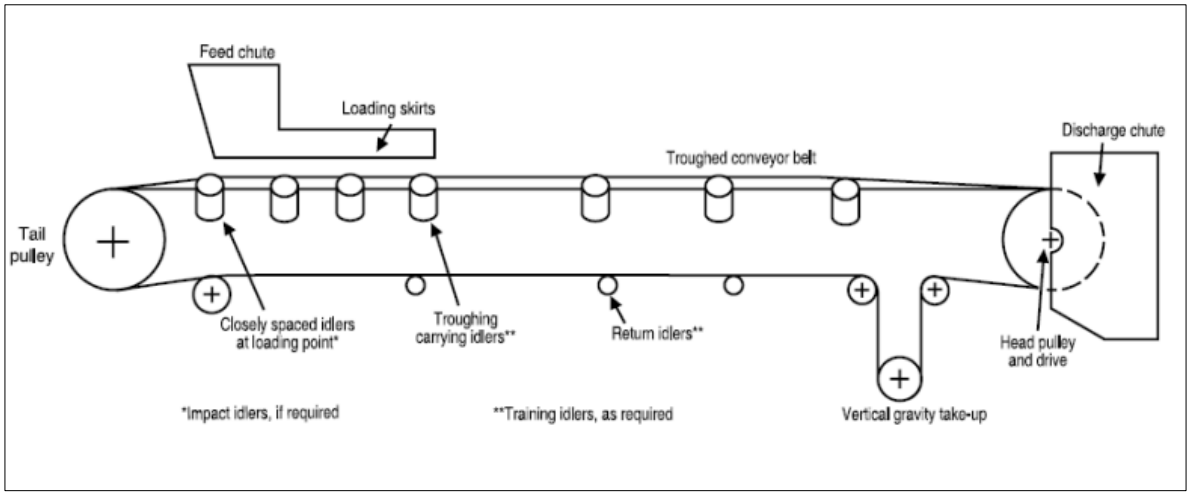

Figure 1–2 Basic drawing of a belt conveyor system [7]

This system consists of two main parts the upper and lower part of the belt which both touch series sets of rollers that are mounted to the conveyor structure itself as stated in Figure 1–3. However at both ends (head, tail) of the conveyor the belt is wrapped around a pulley one of which is coupled to a drive unit to transmit the motion. These systems are characterized by length, loading capacity, velocity, and operating expenses. In LKAB Narvik there are total of 70 belt conveyors of almost 15 km length, having a loading capacity of 9000 t/h for iron ore pellet, and 11000 t/h for fine material [5] the conveyor belt speed in Narvik facility is 3 m/s, with a belt width of 2000 mm, and thickness of 17mm [6].

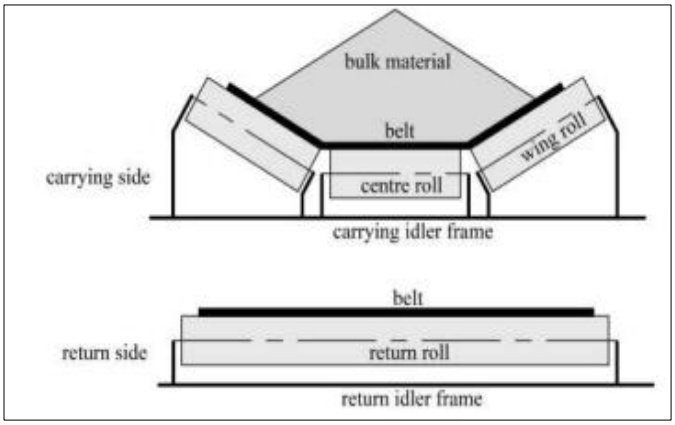

Figure 1–3 Basic drawing of a conveyor idler troughing set [7]

1.4 Problem description

Conveyor rollers at LKAB's Narvik facility, are essential components of the iron ore transportation system, and are posing significant challenges leading to rollers failure and thus requires replacement. Moreover, the replacement of idlers in conveyor systems presents a major maintenance challenge, ranking as the second highest expense after the conveyor belt itself. Therefore, understanding the root causes of idler failure is crucial, given that failures can result from various factors such as exhibiting high loads, wearing of the outer shell of the roller, misalignment of the rollers, and bearing failures. This highlights the importance of conducting thorough inspections and meticulously documenting the causes of replacements. Thus, the need for this master thesis arises from the critical importance of addressing the high replacement frequency and associated failures of conveyor rollers in the LKAB Narvik facility. This master thesis aims to address roller's structural behavior and failure modes, a study for materials used in manufacturing the roller shell, taking into account operational conditions, and maintenance practices to develop targeted strategies that mitigate failures, reduce replacement frequency, and improve overall efficiency.

Additionally, the solution sought should consider the practical aspects of manual replacement, emphasizing factors such as the weight of the components and the accessibility of specific areas within the facility. Also recommend solutions for reducing contaminations in bearing races which in case reduce the bearing failures. Addressing these challenges requires a comprehensive approach that integrates engineering solutions, operational considerations, and ergonomic factors to optimize the replacement process, mitigate failures, and ultimately contribute to the overall efficiency and longevity of the conveyor roller system in the LKAB Narvik facility.

1.5 Project Objectives

This master's thesis addresses the persistent replacement causes of conveyor rollers at LKAB's Narvik facility, crucial for the iron ore transportation system. Through a comprehensive approach integrating engineering solutions, operational considerations, and user-oriented factors, the thesis aims to study the structural integrity of the roller deformations and stresses, extend roller lifespan while optimizing the replacement process within practical constraints. Emphasizing increasing the performance, lifespan, and serviceability, the project investigates

existing challenges and identifies factors contributing to frequent replacements, can be done by performing:

- Structural analysis both static and dynamic analysis for the roller structure.
- Applying material selection procedures to find alternative material and minimizing the roller’s weight.
- Roller bearing analysis.

It also needed to take into account the following design constrains:

- Regulatory compliance where the designed structure should be compatible with the found infrastructure of the conveyor belt in LKAB facility.
- Load constrains where the developed structure should have high strength and a high Young's modulus to withstand the operational loads experienced at the LKAB facility without failure.
- Environmental conditions (Scandinavian weather Conditions)

By focusing on these aspects, the thesis aims to propose innovative solutions that not only mitigate the challenges associated with conveyor roller replacements but also enhance the overall efficiency and reliability of the iron ore transportation system at LKAB's Narvik facility.

Chapter 2: Literature Review

2.1 Overview of Belt Conveyors & Conveyor Idlers

Belt conveyor systems is one of the most critical equipment used by mining industry. A conveyor belt function is to transfer material a variable distance that can varies between few meters to kilometers. Belt conveyors presents many advantages compared to other transportation systems used in bulk material transportations like trucks, and lorry transport. Conveyor system reduces personal costs, energy consumption, and also long period between maintenance, since the system is independent of its surrounding, thus showing cost saving up to 40%-60% [8]. This system composed of several components, few of these components is grouped on the head and the tail of the conveyor belt system such as drive pulley which is responsible for transmitting power to the conveyor belt, tail pulley that serve to maintain proper tension in the belt conveyor, in addition to other tensioning components that are crucial for ensuring proper belt tracking and prevent sagging or excessive slack. However other components are spread along the conveyor belt system causing difficulties in monitoring and servicing [9]. As shown is Figure 1–2 one of the principle component of this system is the elastomer belt which mainly have a dual functions of containing the conveyed material, and transmitting the force needed to move the load [8].

In addition to the elastomer belt, belt conveyor rollers which are cylindrical components strategically positioned along the conveyor frame to provide support for the belt and carry the load of conveyed material, additionally facilitating the movement of a conveyor belt. They are the most important components of this system and represent a considerable value of the whole cost, since they plays a crucial role in the overall functionality and efficiency of the belt conveyor system [8]. Their importance can be highlighted in various aspects of conveyor system operation. Their primary function is to support the belt and they are guaranteed to rotate freely and easily under load. Correct sizing of the roller is fundamental to the guarantee of the plant efficiency and economy in use.

As stated in Table 2-1, there are three main types of belt conveyor idlers. Starting with the carrying idler, this type in installed on the upper frame of the belt conveyor, the main function is to support the belt and load in the transport section of the conveyor. These rollers are manufactured according to specific trough angle (20°, 35°, 45°). However, any other angles are also manufactures upon customer's design and drawings. Second type is return idler which are

installed in the lower frame of the conveyor belt, and also used to support the belt while cycling around to be loaded again. There are several types of return idlers (flat, self-aligning V-shaped, and friction return idler). Coming to the impact idlers that are installed under the loading section of the belt conveyor. They are mainly used to absorb the impacting power of the conveyed materials. In some operations where the impact power is high, these idlers are replaced by something called impact bed [10]. There is one more type of idlers called training idlers that are suitable for use in both return and load carrying side of the conveyor belt. This type is mainly used in reversible conveyors, high load, and slow moving belt conveyors. These idlers can help the conveyor belt running in the right direction.

Table 2-1: Main types of belt conveyor rollers [11]

Main types of conveyor rollers		
 Single- steel carrier	 Single-steel return	 Trough carrier set
 rubber- coated carrier (impact roller)	 rubber disc return	 V-return

Understanding the components of a belt conveyor roller is crucial for optimizing system performance and ensuring reliable operation. A schematic diagram of a belt conveyor roller Figure 2–1 is presented along with a detailed breakdown of its main components in the figure description below. Each component's role will be examined to provide insights into the functionality and importance of the conveyor roller assembly.

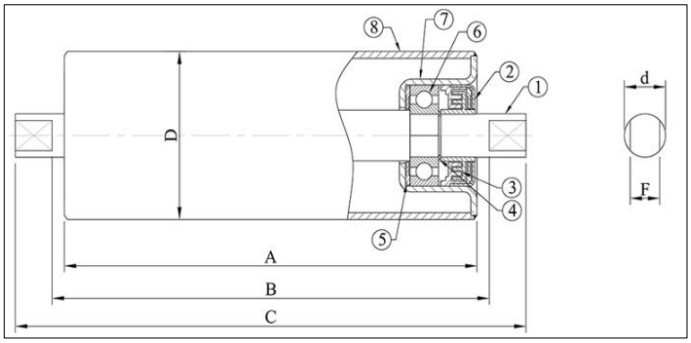

1	Shaft	**5**	Seal	**A**	Roller length	**d**	Shaft diameter
2	End Cap	**6**	Bearings	**B**	Inside Frame Length	**F**	Flats for support slots
3	Labyrinth seals	**7**	Bearing cup	**C**	Shaft length		
4	Circlips	**8**	Pipe	**D**	Roller diameter		

Figure 2–1 Schematic diagram of a belt conveyor roller [12].

- Shaft / Spindle is a rod or axle that runs through the center of the roller, connecting the bearings and providing support for the entire roller assembly.
- End Caps are fitted at each end of the roller and help contain the bearings and shaft within the roller shell.
- Labyrinth seals are a type of sealing mechanism used to prevent the ingress of contaminants, such as dust, dirt, and moisture, into the internal components of the roller, particularly the bearings.
- Circlips are often used to secure various elements of the roller assembly, particularly to hold the bearings in place on the shaft.
- Seals are used to protect the bearings from contaminants such as dust, dirt, and moisture. They help prevent the ingress of foreign particles that could lead to premature bearing failure.
- Bearings are housed within the roller shell and allow the roller to rotate. They play a crucial role in reducing friction between the roller and the conveyor belt, enabling smooth movement.
- Bearing Housing is a compartment within the roller shell that holds the bearings securely in place. It is an essential part of the roller that contributes to its structural integrity.
- Pipe / Shell represent the outer cylindrical surface of the roller, it provide main structure of the roller and support for the conveyor belt.

2.2 Recent Developments in Rollers Technology

Rollers can be classified in term of outer shell material into two main categories: ferrous and non-ferrous rollers. Although non-ferrous rollers are not as popular or versatile as steel rollers, there is an increasing demand for non-ferrous rollers in the industry [13]. The industries that prefer non-ferrous rollers are usually in corrosive environments, such as companies on coastlines or manufacturers that handle corrosive materials like salt. Other companies that are interested in light weight rollers are mines with stacking towers or underground mines. The polymer, composite material roller industry can currently produce rollers up to 535 mm in length and various diameters [13]. The call for larger, light weight rollers (such as 1200 mm in length and 150+ mm diameters) in the market remains unfulfilled. There are various designs and configurations based on the specific requirements of the conveyor system and the material being transported, and according to specific challenges in diverse industrial application [13].

RULMECA the Italian company is one of the companies that design and manufacture belt conveyor rollers and troughing sets. They are specialized within bulk material handling industry, with two main types of rollers classified according to material (ferrous, and non-ferrous material). Rulmeca modern roller technology are PSV Mono-block rollers designed for heavy duty conditions these rollers are available with shaft diameters from 20mm to 40mm having a robust steel construction and an hermetic sealing system as shown in Figure 2–2 [8]. This design provides extremely high load capacity and resistance to impact, corrosion and abrasion of bulk materials, pollutants and other aggressive elements during conveyance. PSV rollers is defined as between -20°C and + 100°C with standard greased components, offering maximum effectiveness and productivity, furthermore combined with commonly desired energy savings, long working life and minimal maintenance over time. The characteristic of a mono-block is that the bearing housings of the PSV rollers are welded to the tube body [14].
In RULMECA there are two main executions for bearing protection contactless, and hermetic. The contactless configuration is recommended where a very low resistance is preferable or requested, with outdoor normal environmental conditions [14]. Thus the external wiper seal is not available. However in hermetic execution as shown in Figure 2–2 is recommended in presence of rain, water, salt water, high humidity, powder, sand, dust or dirty applications in general.

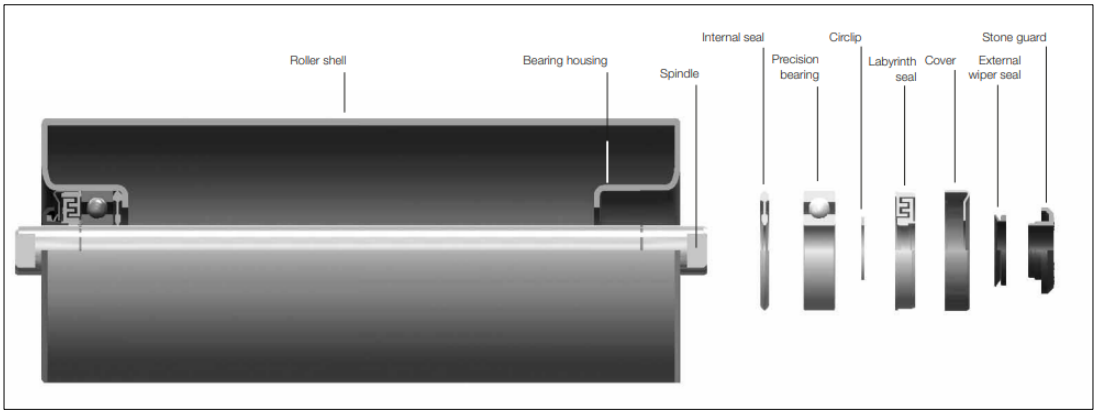

Figure 2–2 Rulmeca PSV-hermetic roller internal components [8].

Similarly, Superior Industries and other companies like MESTO the Swedish company, that have a manufacturing membership of CEMA (Conveyor Equipment Manufacturers Association) following CEMA standards, and safety recommendations for designing and manufacturing conveyor belts equipment, manufacture several classes of CEMA rollers. Figure 2–3 below represents the Moxie rollers which are mainly HDPE (high density polyethylene) which are designed to function in extreme weather conditions, corrosion resistance), 50% lighter than the steel rollers which reveal in reduction of power required to driven these belt and also lighter load for the maintenance crew. Moreover Moxie rollers generates 3 times less noise that the steel ones [11].


Figure 2–3 Superior Industries Moxie rollers [15].

Moreover, DYNA Engineering, responsible for manufacturers and suppliers of conveyor belt equipment's and services. The manufacturer come out with an idea of rubber coated roller, where rubber is vulcanized directly to the pipe. The key features of rubber coated rollers is that these rollers resist tearing, pounding and friction which increase the life span of the roller.

As shown in Figure 2–4, RKM Company invented a heavy duty lightweight composite roller. This composite roller is manufactured by processing high grade glass reinforcement and resin

to bind the fibers together [16]. This composite combination have been used in several applications such as piping, road bridges, Pontoons, and various mine structures. The result was a high flexural strength and stiffness roller compare to steel, up to 50% lighter, advanced wear properties, and high performance sealing set. For the sealing RKM have designed a heavy duty nylon protective outer dual labyrinth shield as shown in Figure 2–4 below, which will eliminate any rock jamming and provide additional protection from contamination [16].

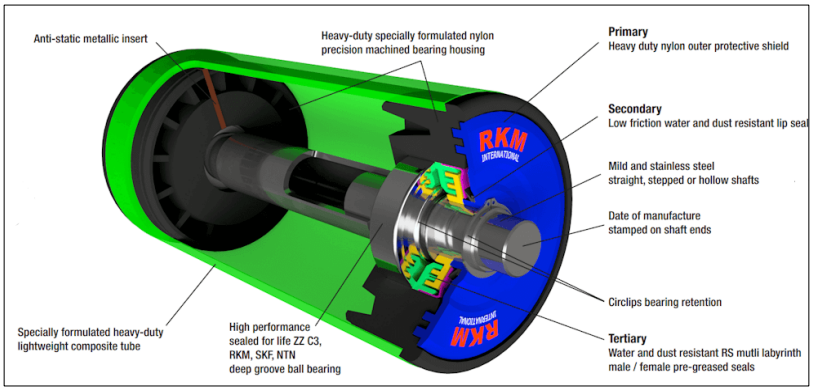

Figure 2–4 RKM heavy duty lightweight composite roller [16].

Another type of rollers was also manufactured and produced by RKM the Australian company is the Medium Duty PVC Roller – Low Noise Anti-Static Roller.

Figure 2–5 shows the shell body of the roller is PVC (Polyvinyl chloride), which make it lighter, corrosion resistance, also having low friction coefficient which reduces the amount of material stuck to the roller body. Moreover this type of rollers contains an Anti-static copper insert to protect the components from electrostatic discharge. Note that this type of roller is mainly used as a return roller [16].

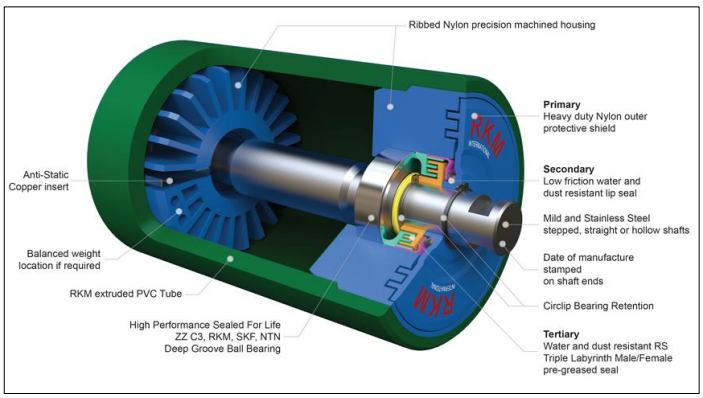

Figure 2–5 RKM medium Duty PVC Roller – Low Noise Anti-Static Roller [16].

Now, turning our attention to Figure 2–6, we observe that the bearing housing itself is constructed from heavy-duty solid poly precision or ribbed nylon precision materials. The bearings utilized in this roller type are high-performance sealed-for-life ZZ C3 RKM SKF, NTN deep groove ball bearings. These bearings are safeguarded by male/female triple labyrinth pre-greased seals, all enclosed within a steel shield. Furthermore, an outer shield made of heavy-duty nylon provides additional protection for the entire seal package.

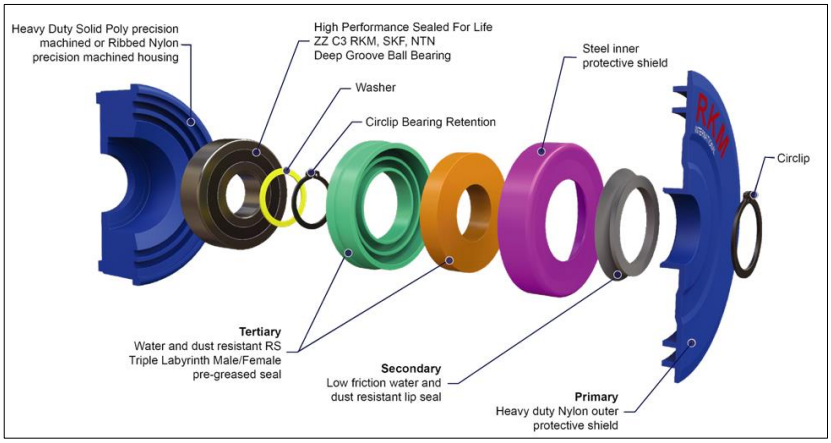

Figure 2–6 exploded RKM composite roller seal package [16].

2.3 Standards and Regulations in Conveyor Idler design

Before the establishment of standards, each idler manufacturer produced idlers with distinct dimensions and fixing arrangements. However, over time, users, who had installed idlers from different manufacturers on various conveyors, found themselves obligated to maintain a diverse collection of non-interchangeable idlers and spare rollers in their inventory for maintenance purposes. This situation led to considerable inventory costs and expenses arising from changes in critical dimensions over time [17].

Thus, standards for conveyor belt idlers play a pivotal role in maintaining uniformity in design and manufacturing practices within the industry. One prominent organization dedicated to this cause is the Conveyor Equipment Manufacturers Association (CEMA), which establishes comprehensive standards guiding the design, production, and application of conveyor equipment, including idlers. An illustrative example is CEMA Standard 502-2019, titled "Bulk Material Belt Conveyor Troughing and Return Idlers," [18] a significant benchmark within the CEMA framework. This standard furnishes specific directives for designing and manufacturing troughing and return idlers, encompassing critical dimensions, load-bearing capacities, and

prescribed testing procedures that manufacturers must adhere to during the production of these indispensable conveyor components. Moreover, CEMA places substantial emphasis on design considerations, underscoring factors like idler spacing, material characteristics, and load capacity. These guidelines serve to ensure that idlers are engineered with the requisite structural integrity to effectively withstand operational stresses.

Internationally, the International Organization for Standardization (ISO) contributes to the formulation of conveyor idler standards. ISO 5048 [19], for instance, presents a comprehensive framework for conveyor belt design, inclusive of considerations for idlers within the broader conveyor system. This standard covers parameters such as belt speed, belt width, and idler geometry, fostering a global approach to the design and manufacturing of conveyor systems.

In specific regions, organizations like the German Institute for Standardization (DIN) exert influence over design and manufacturing practices. DIN standards, exemplified by DIN 22101, address aspects of belt conveyor design, potentially incorporating considerations for idler specifications in alignment with German engineering practices. Similarly, South African Bureau of Standards (SABS 1313) [20] SANS 1313-1:2008: This South African National Standard specifies requirements for rubber or plastics-covered conveyor belting of textile construction for underground mining on flat or troughed idlers, the British Standards Institution (BSI) BS 2890:1989 [21], which addresses troughed belt conveyors. While encompassing broader aspects of conveyor systems, it includes specific considerations for idlers, setting requirements for their design and construction, and the Japanese Industrial Standards (JIS) JIS B 8803-1990 focuses on the general specifications for idlers and idler sets used in belt conveyors [22]. It covers dimensions, design features, and performance requirements, providing guidelines for the manufacturing and application of conveyor idlers.

To summarize, strict adherence to standards such as CEMA, ISO, and local standards like DIN, SABS is indispensable in the meticulous design and manufacturing of conveyor belt idlers. These standards serve as a bedrock for ensuring consistent quality, safety, and performance throughout the conveyor industry. Staying well-informed about these standards is imperative for manufacturers and engineers to uphold the highest standards of excellence in conveyor system components.

2.4 Inspection Procedures and Failure Modes in Rollers

Understanding the reasons behind idler replacements is crucial, given that they constitute the second highest maintenance expense in the transportation process, following the conveyor belt itself which accounts around 30% to 70% from the maintenance cost [23]. Rollers may fail due to several causes, however the primary reasons for replacement was detected upon analyzing the information gathered on 97,778 idler rollers, operating in belt conveyor used to transport ore material, the reasons were as follows: Noise/Vibration, Seizure, Wear, high temperature, Broken, Standardization [23]. According to the survey, the most common reasons for replacing carrying and impact rollers are noise, wear, and seizure, which account for almost 90% of replacements. Notably, noise is more relevant in carrying rollers, but for return rollers the primarily replacement causes is due to wear, noise, and standardization, accounting for approximately 90% of all replacements in this category [23].

In summary, impact and carrying rollers generate more noise due to heavier loads, while return rollers wear quickly from contact with the abrasive belt. Lateral rollers follows replacement parameters: noise, seizure, and wear, contrasting with central rollers, where wear is the second most common reason for replacement. This is due to the exposure of external bearings of side rollers to environmental factors, leading to decreased lubricating grease efficacy and increased seizure failures. Additionally, central rollers, bearing heavier loads, operate at higher temperatures, requiring more repairs than side rollers [23]. On the other hand, another research performed by Konig and Oepen in (2013) [24] at an RWE mine in Germany shows that the two most important failure modes of carrying wing idler operating at Hambash mine (brown coal mine) in 2007 and 2012 are considered to be bearing failure lagerschaden (red) and shell failure mantelverschleiss (blue) Sonstiges represent other types of damage (green) shown in Figure 2–7. This implies that significant part of roll failures that had been reported is caused be either bearing failure or by roller shell wear. Moreover what can be concluded from Figure 2–7 is that within these two failure modes the consequences of bearing failure is more dominant, and the rate of shell wear will be accelerated if one of the bearing runs into seized state.

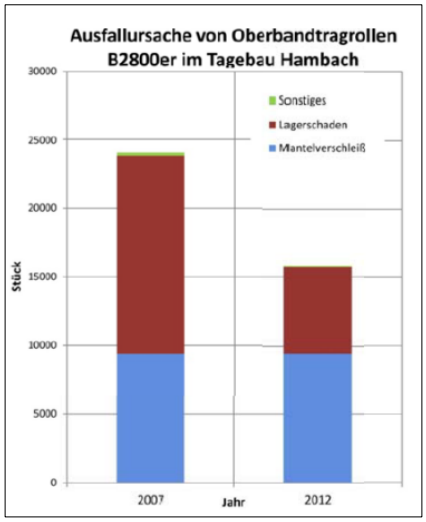

Figure 2–7: Failure modes of belt conveyor rollers [24].

The reason behind bearing failure can be contamination, lack of lubrication, or over-loading, however contamination is a major factor that influences the actual life time of the bearings [24]. These contaminants can be present in liquid or solid state according to the operation conditions. Thus having an effective sealing system is important to protect the bearing and increase the operation life, since when this system in malfunctioning it fails to prevent the contaminants from accumulating around the bearing and thus bearing failure occurs. Also significant deflection of roller shaft, or misalignment can contribute additional radial and axial force to the bearings leading to failure [25].

In summary, conveyor rollers face mostly three main failure modes: noise (vibration), bearing failure, and shell surface wear, impacting operational efficiency, reliability, and maintenance costs. Excessive noise, often a result of vibration, indicates potential performance and structural issues [26]. Moreover, Bearing failures cause costly downtime and material transportation disruptions. Addressing these challenges requires selecting durable materials and implementing effective maintenance strategies to enhance roller lifespan and minimize operational disruptions, crucial for improving conveyor system performance across industrial applications.

2.5 Load Distribution Characteristics in Conveyor Idler

Analyzing load distribution in a roller idler is essential for understanding its behaviour under various loads. The configuration of troughing idlers determines the load distribution profile, with the load evenly applied to the center idler due to uniform material distribution in that area, while wing idlers experience non-uniform load distribution. This discrepancy implies that the central roller undergoes greater stress than the wing rollers. Conversely, the inner end of the

wing roller experiences higher stresses than the outer end, which is predominantly exposed to external environmental factors like rain, snow, and sunlight, potentially increasing the risk of bearing damage or wear. Moreover, calculating stress distribution involves certain assumptions and considerations. A key assumption is the homogeneity and uniform flow of ore material, leading to a load distribution profile resembling that illustrated in Figure 2–8. Additionally, parameters influencing this calculation include the troughing angle, bearing sizes determining axial and radial bearing loads, belt initial weight, and the idler weight.

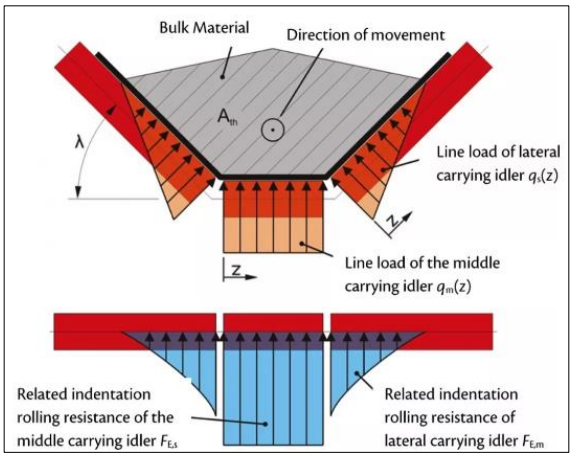

Figure 2–8: Schematic diagram of load distribution among center, wing idler [27].

It's important to mention that from the industrial practice for the selection of idler rolls, it can be concluded that a precise determination of the load on idler rolls is still missing. The load sharing factors provided by industrial standards are rather rough estimations. Idler rolls which are selected according to such estimation often experience premature failures due to excessive loading [28]. Table 2-2 shows two different assumptions for the load sharing factor by two different manufactures CEMA to the left, and Rulmeca to the right [8].

Table 2-2: Sharing factor of central idler with respect to trough angle.

Trough angle (°)	Load factor
20	0.722
35	0.778
45	0.80

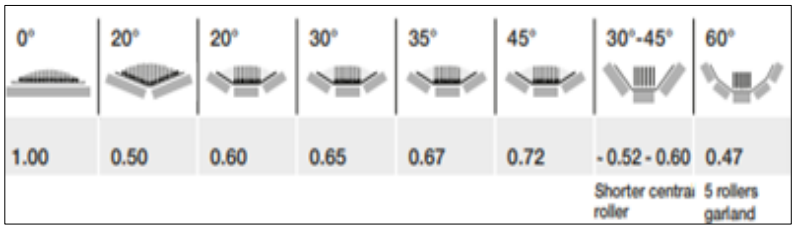

Furthermore, the uneven distribution of load between the wing rolls and the center roll results in varying lifespans, posing challenges in monitoring and replacing rolls. In certain industrial procedures, batches of idler rolls are replaced simultaneously. This can result in waste of wing rolls which are still in good conditions if decisions on roll replacements are based on the condition of center rolls. On the other hand, severe center roll failures may occur if decisions on roll replacements are based on the condition of wing rolls. Thus, it is important to have good monitoring for operating idlers. Note that these assumptions may vary among manufacturers, and additional parameters might be considered in load distribution calculations.

Chapter 3: Design Methodology

This chapter outlines a systematic approach to address the challenges of designing belt conveyor rollers for harsh conditions in a Scandinavian iron ore transportation facility in Narvik. It encompasses a structured sequence of steps and considerations aimed for ensuring the successful design of robust, efficient, and durable conveyor rollers, taking into account environmental conditions, operational requirements, and performance expectations of the idler system. Virtual prototyping analysis, including static structural and dynamic modal analysis, will be conducted and discussed to estimate the stress distributions, deformations, among roller's shell and shaft. Modal analysis is used to estimate the modal frequencies and mode shapes of the studied roller. Moreover, material selection follows Ashby's method for identifying materials aligned with project objectives and constraints, ensuring optimal performance in wear resistance, corrosion resistance, and low-temperature conditions is performed. In addition, to the previous analysis bearing component of the roller undergo an explicit study for estimating the lifespan. Finally, proposing solutions that can reduces contaminations accumulation in bearing race is discussed.

3.1 Design Specifications and Calculations for Conveyor Idlers

A well-developed design specification table is essential for ensuring the success of a design project by providing clear guidance, ensuring quality and compliance, managing risks, and facilitating effective communication among stakeholders. Table 3-1 shows the design parameters that must be taken into consideration during design process. In addition, design specifications establish the structure for defining design parameters and constraints, while calculations evaluate the practicality of meeting these specifications and guide design adjustments. Moreover, as the design progresses, specifications may undergo refinement or modification in response to calculation outcomes, ensuring alignment with the intended goals of the final product.

Table 3-1: Design specifications of conveyor belt idler.

Design Specification	**Description**
Application	Idler roller of a belt conveyor system for transporting iron ore in harsh environmental conditions.
Material	High strength capable for withstanding material loads
	High stiffness experience low deflections
	Wear resistance resisting wear and tear over prolonged use
Center roller length, shell diameter, and shaft diameter	(950mm, 194mm, 40mm), respectively.
Side roller length, shell diameter, and shaft diameter	(600mm, 157mm, 30mm), respectively
Bearing type	6306, 6308 rubber shielded, internal clearance CN (Normal clearance) [29].
Bearing housing	Deep-drawn quality sheet steel, M7 bearing seat, C3 to C4 clearance [8].
Roller Load capacity	Able to handle 9000t/h conveyor load capacity.
Environmental conditions	Resistant to: corrosion, moisture, and extreme temperatures.
Operating temperature Range	-40°C - 40°C
Weight	50% mass reduction for enhancing maintenance procedure.
Compliance	Meets LKAB standards and regulations.

Upon grasping the design specifications, it becomes essential to outline the specific properties of the conveyed material, exemplified here by iron ore pellets. These characteristics are detailed in Table 3-2 ranging from particle size, shape, and density to abrasiveness and flow ability. Furthermore, additional attributes such as material slope characteristics ‘angle of repose’ and ‘angle of surcharge’ are subsequently expounded according to specific standards provided by CEMA. Angle of repose is the steepest slope of the unconfined material, measured from the horizontal plane on which the material can be heaped without collapsing [30]. However, angle of surcharge (As) shown Figure 3–1 represents the inclination of material relative to the horizontal plane when it's in motion or being agitated, such as when conveyed on a moving belt. A greater surcharge angle indicates a higher capacity for material accumulation on the belt.

Table 3-2: Characteristics of bulk solid material according to CEMA standards.

Material description & density	Iron Ore, Pellets / $(3\ t/m^3)$
Size	Granular- Under 1/2 *inch*
Flow-ability /Angle of repose	Average flow angle of repose 30°-39°
Angle of Surcharge (α)	25◦
Maximum Allowable angle of conveyor inclination	13°-15°
Abrasiveness	Very abrasive
Miscellaneous Characteristics	Very dusty-Highly corrosive

Understanding these material properties is crucial for optimizing the design of an effective conveyor idler capable of efficiently handling and transporting the conveyed materials.

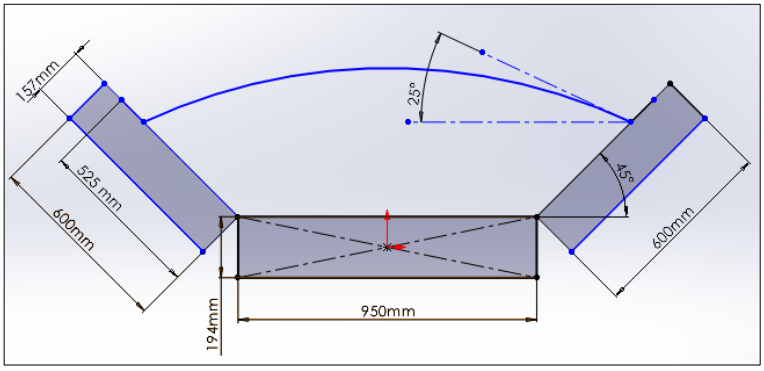

Figure 3–1 Schematic diagram showing area of load cross section between two idlers.

Figure 3–1 shows the cross-section between two idlers, depicted in SolidWorks, reveals differences between wing and center idlers. According to the drawings provided by LKAB, wing idlers have a troughing angle of 45° with the horizontal. These wing idlers measure 600mm in length and have a diameter of 154 mm. In contrast, the center idler is 950mm in length with a diameter of 197 mm, indicating variations within the idler set under study.

The initial parameter required to compute the load exerted on the idler assembly is the conveyor belt's load capacity. This metric considers various factors such as the dimensions (length) of both central and wing idlers, belt width, and conveyor belt velocity. The load capacity signifies the mass flow rate of material that the conveyor belt can accommodate, thereby enabling the calculation of load distribution across the idler assembly. In the examined scenario, the conveyor belt's load capacity is specified as 9000 tons per hour. However, in the absence of this

value, computations regarding the material's occupied area must be conducted to determine the load capacity $\dot{m}$ using the following equation:

$$\dot{m} = Av\rho, \tag{1}$$

where:

ρ: conveyed material density (Kg/m^3).

v: conveyor belt velocity (m/s).

A: area occupied by the material (m^2).

Figure 3–2 shows a method for calculating the occupied area by conveyed material of three identical idlers. However, in the studied case the idlers are not identical and thus the calculations will be more complicated.

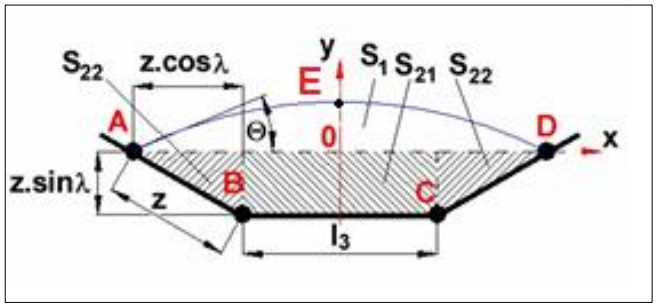

Figure 3–2 cross-sectional area of a belt conveyor with a three idler set [31].

As stated in [31] the total area is denoted by S, the cross-section of the load consists of a trapezium ABCD and a segment of a circle AED as shown in Figure 3–2

$$S = S_1 + S_2\,. \tag{2}$$

S_1:Represent the area bounded in the section (AED) as shown in Figure 3–2 and can be calculated according to the given equation [31]:

$$S_1 = \frac{1}{2}\left(\frac{2z\cos\lambda + l_3}{2\sin\alpha}\right)^2 \times \frac{2\pi\alpha}{180} - \sin 2\alpha\,, \tag{3}$$

where:

λ: trough angle (°).

l_3: central idler length (m).

z: length along wing idler to the limit of the load (m), represented as follows [31]:

$$z = \frac{B}{2} - \frac{l_3}{2} - x\,, \tag{4}$$

$$x = 0.005B + 0.025\,, \tag{5}$$

B: belt width (*m*)

x is a correction constant to approximate the load limit.

Similarly, for calculating the area S_2 bounded in section (ABCD) [31]:

$$S_2 = S_{21} + 2S_{22}\,. \tag{6}$$

$$S_2 = z\,sin\,\lambda\ (l_3 + z\,cos\,\lambda)\,. \tag{7}$$

Thus the total area *S* (ABCDE) [31]:

$$S = \frac{1}{2}\left(\frac{2z\,cos\,\lambda + l_3}{2\,sin\,\alpha}\right)^2 \left(\frac{2\pi\alpha}{180} - sin\,2\alpha\right) + z\,sin\,\lambda\ (l_3 + z\,cos\,\lambda)\,. \tag{8}$$

Finally, after calculating area given by equation (8) we apply equation (1) to calculate mass flow rate then apply equation (9) to get belt load capacity.

Calculating the total weight acting on the conveyor knowing that this load is due to two main factors: the material that is being conveyed, and the weight of the conveyor belt itself. Weight of material Q in kg/m, knowing that the load capacity C of the conveyor belt is given to be 9000 t/h, and the belt velocity v is 2.9 m/s, simply divide the load capacity by conveyor velocity:

$$Q = \frac{\dot{m}}{v_{belt}} = 862Kg/m\,. \tag{9}$$

Moreover, LKAB's belt specifications given in TR010 drawings refer to Appendix A show that the total mass of the belt is 84395 Kg with a length of 1257+m [32], thus to calculate the weight/meter divide the total mass by the total length.

$$m_{belt} = \frac{M_{total\ belt}}{Length_{belt}} = 67.14\ \text{Kg/m}.$$

Adding this weight to the material weight calculated before we get the total weight acting on the idlers. Therefore, the total static load acting along 1 meter of conveyor belt is calculated according to the following equation:

$$F_{total} = 9.81\left(Q + m_{belt}\right) = 9115\ \text{N/m}. \tag{10}$$

Thus resultant total static load found to be 9115 N, acting on one meter. Knowing that this load is to be multiplied by the spacing distance between the idlers which is 1.2 m, therefore the resultant total static load acting on 2 sets of idlers is:

$$F_{total\ (1.2m)} = 1.2F_{total} = 10940\ \text{N/m}.$$

Assuming that this load is only acting on the idler sets then 10940N is to be divided on the two idler sets. As mentioned in Table 2-2, participation factor/load factor ($F_{P-center}$) at the center idler is in the range between 0.6-0.80, in the studied case CEMA standards will be used $F_{P-center} = 0.80$

$$F_{center\_distributed} = F_{P-center}\ \frac{F_{total(1.2m)}}{2} = 4.38\ \text{N/mm}\ .$$

Similarly the forces acting on the wing (side roller) will be evaluated accordingly:

$$F_{wing} = \frac{(1 - F_{P-center})\ \frac{F_{total(1.2m)}}{2}}{2} = 0.55\ \text{N/mm}\ .$$

Considering the hypothetical scenario where the load distribution on the center idler is assumed to be uniform, and positing a non-uniform load distribution for the wing (side) roller, characterized by a triangular distribution with maximum intensity decreasing from maximum towards null at the belt edge.

3.2 Static and dynamic Analysis of Roller Shells and Shafts

3.2.1 Analytical Calculations

In context of conveyor idlers, static structural analysis is crucial in assessing the idler's ability to withstand static loads and maintain structural integrity under steady-state conditions. Thus, a static structural analysis will be done for both idler shell, and the shaft, and for verifying the analysis solution analytical calculation will be done to ensure the validity of the results.

The distribution of forces along the shaft, roller shell, and supports is illustrated in Figure 3–3. It demonstrates that the roller shell experiences a uniformly distributed load resulting from the combined weight of the belt and conveyed material assuming that this load is rectangular distributed load. However, for simplicity this distributed load is assumed to be a point load acting in the center of the roller. For the shaft the resultant of this distributed load is then

transmitted to the shaft, where it is concentrated into two point loads at the bearings. Additionally, the shaft is securely fixed at both ends to support the applied loads effectively.

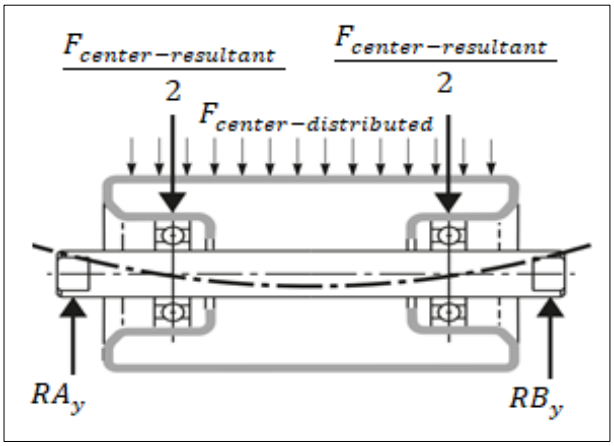

Figure 3–3: Loads acting on the central idler assembly [24].

Moreover, Figure 3–3 helps in applying the support conditions for the roller and the shaft. By running the static structural analysis, maximum deflection and stress distribution, bending moment and shear force diagrams are obtained. Moreover, for verifying numerical results. Analytical calculation of the deflection and stress – distribution for both roller shell, and shaft respectively. For this means Euler Bernoulli beam theory is used to calculate the maximum deflection due to bending in cylindrical shell under point load.

Roller shell doesn't exhibits any displacement, and moments in (*x*, *y*,and *z*) directions [34]. Thus, it is assumed that the roller shell is fixed supported at both sides.

Maximum deflection of shell can be calculated by:

$$\delta_{shell-max} = \frac{5F_{Center}\,L^3}{384EI_{y-shell}}, \tag{11}$$

where:

F_{center} : is the resultant of the distributed load acting on the center of roller (N)

E: material's Young's modulus (stainless-steel 195 GPa.)

$I_{y-shell}$: moment of inertia of the roller shell cylinder (m^4), and can be calculated using the following equation:

$$I_{y-shell} = \frac{\pi}{4}(r_{outer}^4 - r_{inner}^4), \tag{12}$$

where:

r_{outer} , r_{inner}, are the outer and inner radii of the roller shell (m).

The maximum bending moment can be calculated using the following equation:

$$M_{max} = \frac{F_{Center}\, L}{8}, \tag{13}$$

where M_{max} is the maximum bending moment (Nm).
The maximum bending stress in the roller shell is represented as follows:

$$\sigma_{max} = \frac{M_{max}\, y}{I_{y-shell}},$$

where *y* is the distance from neutral axis to the top or the bottom of the shell is this radius (m).

A minimum thickness of the shell can be obtained with a goal to keep the angular deflection not exceeding 0.004 radians required for the proper functioning of deep groove ball bearings [35], and it is calculated by the following equation:

$$y_{shell} = \frac{F_{center\_distributed}\, L^3}{24 E I_{y-shell}} \tag{14}$$

Table 3-3: Analytical calculations for the center rollers.

	Maximum Deflection (mm)	**Maximum Bending Stress (MPa)**	**Deflection Slope (radians)**
Center Roller	1.45×10^{-2}	2.9	4.415×10^{-5}
Wing Roller	1.35×10^{-3}	0.27	1.254×10^{-6}

The analytical calculations of the center, and wing idler shows that center idler exhibits a maximum deflection of 1.45×10^{-2} mm, at the middle of the roller, with a maximum bending stress of almost 3 Mpa. Moreover, the side idler's maximum deflection, and stresses are 6.67×10^{-4} mm, and 0.27 MPa, which are way less than the center roller. Moreover, the condition for deflection slope is satisfied in for both cases and it is stated in Table 3-3. These results were expected, since wing roller is facing lighter loads in comparison to the center roller. These findings shows that wing idler doesn't have high structural influence on the idler set.

Establishing the deflection of the shaft is important to ensure the safe, dependable, and effective functioning of the conveyor system, thereby extending its longevity and diminishing maintenance requirements. Figure 3–4 illustrates the free body diagram of the examined shaft, featuring the requisite dimensions essential for computing the maximum deflection of the shaft under the imposed loads and constraints.

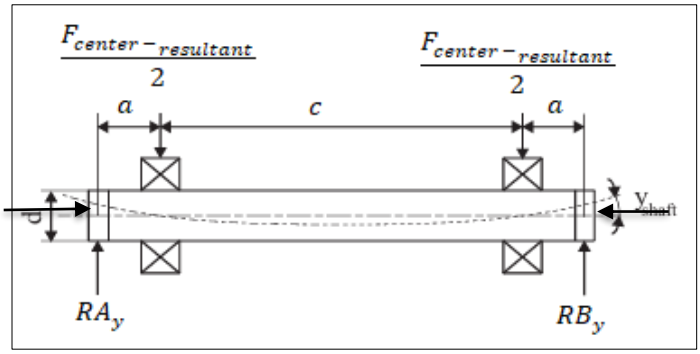

Figure 3–4: Shaft free body diagram [24].

Similarly, the shaft deflection along the force direction, and angular deflection is calculated using equation (15), and (16), respectively [34].

$$\delta_{shaft} = \frac{F_{center-resultant} a^2 (3L - a)}{6EI}, \quad (15)$$

$$y_{shaft} = \frac{16 F_{Center-resultant} (a^2 + ac)}{\pi E d^4}, \quad (16)$$

where:

δ_{shaft}: shaft deflection (m),

y_{shaft}: shaft angular deflection (radian),

$I_{y-shaft}$: shaft moment of inertia (cylindrical cross-section) (m^4),

a: distance from shaft end to bearings midpoint (m),

b: distance between the two bearing midpoints (m),

d: shaft diameter (m),

It is important to mention that the basis for any structural calculation is to calculate the reaction of the supports. An explicit analytical calculation for the wing idler supports is mentioned in Appendix B: Supplementary Study. This calculation shows that the loads acting on wing roller aren't significant compared to that of center roller. Similarly findings stated in Table 3-4 indicates that the values of deflection of wing idler aren't that significant. Thus, it was decided to neglect the wing idler from the remaining finite element analysis study chapter 3.2.2.

Table 3-4: Analytical calculations for shaft deflection and deflection.

	Center (982mm,40mm)	Wing (632mm,30mm)
Deflection (mm)	3.88×10^{-2}	5.58×10^{-3}
Deflection Slope	3.16×10^{-3}	8.40×10^{-8}

The analytical results presented in Table 3-4 outline the maximum deflection values for both the idler shell and shaft in both center and wing cases. Notably, the center idler shell, and shaft exhibit higher deflection values which are 1.45×10^{-2} mm, 3.88×10^{-2} mm respectively compared to wing counter parts which are $1.35 \times 10^{-3} mm$, and $5.58 \times 10^{-3} mm$ respectively. This indicates that the center idler experiences greater deformation, likely influenced by higher load distribution, due to the fact that around 80% of the material weight is distributed on the center idler. Similarly, for the angular deflection outcomes for the center configuration are greater than that of the wing configuration. This observation highlights contrasting rotational behaviours between the two configurations mainly influenced by the load distribution and geometric configuration. The slope deflection should not exceed 0.004 radians, required for the proper functioning of deep groove ball bearings [35], the roll shells should be thick enough not just to guarantee maximum tolerable deflection under the load, but also to survive the long term wear till the end of the lifetime of the roll.

3.2.2 Finite Element Analysis (FEA)

3.2.2.1 Static Structural Analysis

For results confirmation, and visualization of the structure behaviour, static structural analysis was conducted using Ansys Workbench. The setup of the analysis, including the selection of materials, mesh size determination, definition of boundary conditions, and application of loads, was systematically performed. Detailed procedures with figures and tables for clarity and reference for each of these steps, and assumptions considered to run the analysis are provided in Appendix A. Analysis was done on both roller shell, and shaft separately.

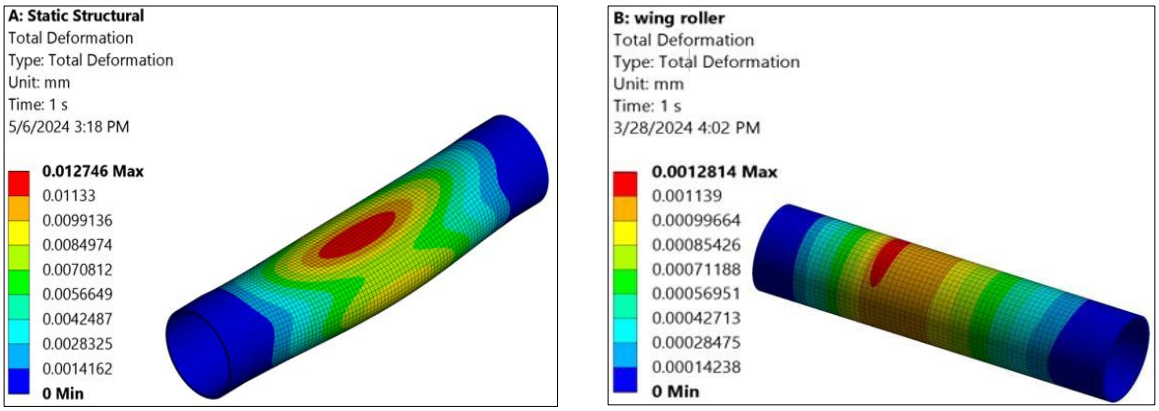

a) b)

Figure 3–5: Total deformation of shell a) Center idler, b) Wing idler (mm).

Figure 3–5 shows that the center idler recorded a maximum deformation of 0.012746 mm, mainly concentrated at its midpoint, greater than that of wing idler which shows a maximum of 0.00128 mm due to the fact that the center idler is experiencing higher loads than the wing idler. These deflection values shows a percentage of error of 10% from the theoretical calculations that shows 0.0145 mm maximum for center idler, however still acceptable since errors may occurs in simulations due to assumptions taken, meshing sizes, and type, and other software limitations.

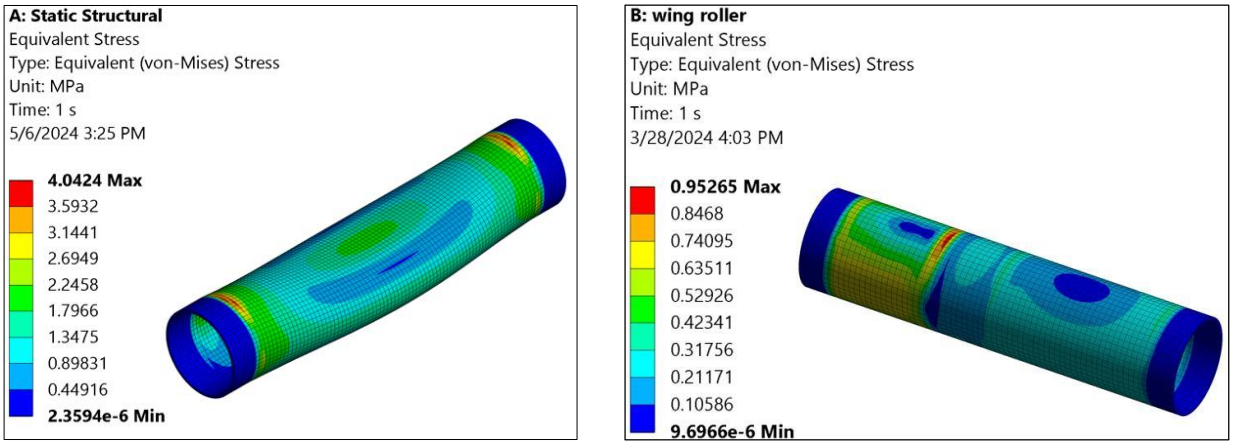

a) b)

Figure 3–6: Von-misses stress distribution among shell a) Center idler, b) Wing idler (MPa).

Moreover, Figure 3–6 reveals that stress distribution within the central idler shows maximum of 4.0424 MPa, with the highest stress concentration observed at the bearing housing ends, suggesting a potential section in the idler's structural integrity. Conversely, the stress distribution in the wing idler varies between 0.53 MPa and a maximum of 0.95 MPa, with the highest stress recorded in the lower section of the idler due to material accumulation, leading to non-uniform load distribution. It is important to mention that despite these stress concentrations, the maximum stress values remain insignificant when compared to the material properties of steel, emphasizing the overall robustness of the idler design.

Furthermore, upon comparison the deformation of the roller shell, it is evident that the shaft exhibits higher deformation values as shown in Figure 3–7, reaching 0.04148 mm. This can be attributed to which the distributed load on the roller shell is transferred to a point load on the shaft. Furthermore, the examination of the moment of inertia of both the roller shell and the shaft corroborates the following findings. According to the deflection formula, there exists an

inverse relationship between deflection and moment of inertia: as deflection increases, moment of inertia decreases, and vice versa.

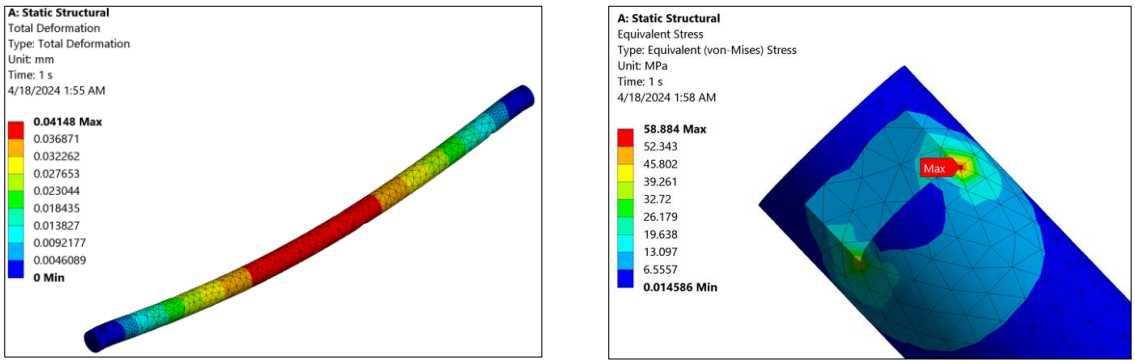

a) b)

Figure 3–7: Center shaft a) Total deformation (mm),b) Von-misses Stress distribution (MPa).

Moreover, examining the stress distribution within the shaft, it is evident that the highest stress, reaching almost 60 MPa, occurs at the attachment point where the shaft connects to the idler's structure. This high stress level is primarily attributable to the non-uniform geometry presented at this juncture, which also should be taken into consideration upon optimizing the structure.

Structural Analysis Results Discussion

Analysis done in Ansys workbench shows relatively high error percentage between theoretical and numerical analysis especially in stress values. Thus, a decision was made to conduct further analysis using Ansys Mechanical APDL, for verifying the results of center roller shell analysis. Same assumptions that were considered in the previous analysis are used in this analysis, and experimental set-up is shown in Appendix A.

Upon running the analysis in Ansys APDL, it is needed to create the bending moment, and shear force diagrams to indicate whether the results matches the theoretical calculations. As shown in Figure 3–8, the moment distribution varies from -468 N.m on the ends of the roller and shows a maximum value of 468 N.m at the midpoint of the roller, which almost equal to the theoretically calculated maximum bending moment. Similarly for the internal shear force value where it shows 2080 N, which also match the theoretical calculations where the reaction force in y-direction is 4160 N divided on both sides.

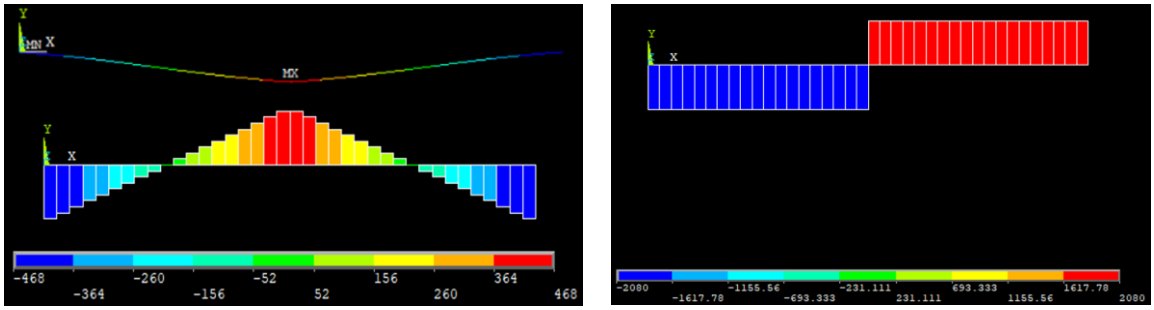

a) b)

Figure 3–8: a) bending moment diagram (N.m), b) shear force diagrams (N) center roller.

After insuring that the analysis results of the forces match the theoretical results it is possible to check the results of deflection and stress distribution among the roller shell. Figure 3–9 shows that the maximum deflection is 0.013 mm, centered in the middle of the roller which is similar for that obtained in the previous analysis. However, for stress values, stress distribution given by Ansys APDL analysis reveals the maximum stress σ_{max} is 2.7 MPa as shown in Figure 3–9. σ_{max} is almost equal to that calculated theoretically, unlike the obtained results of Ansys workbench software.

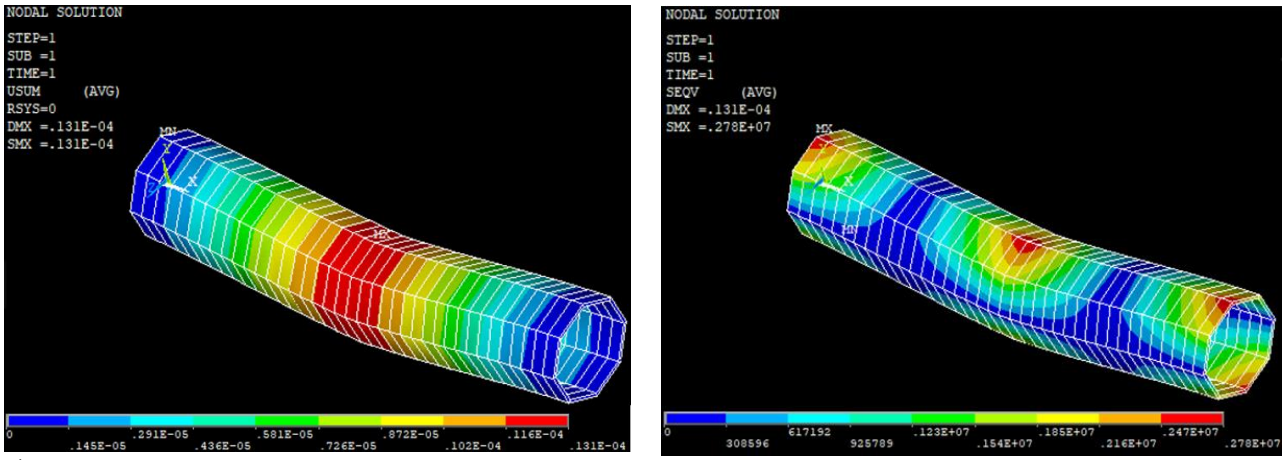

a) b)

Figure 3–9: a) Total deformation (m), b) stress distribution (Pa) center idler APDL analysis.

The fact that the stress distribution from Ansys Mechanical APDL closely matches the theoretical calculation while differing from the results obtained from Ansys Workbench software implies that the choice of analysis software and the methodology can significantly impact stress predictions. This variation underscores the importance of thorough validation and verification processes in structural analysis to ensure accurate and reliable results.

Moreover, validation in (FEA) compares simulated results with real-world measurements from physical experiments, ensuring accuracy. It verifies that analysis methods, assumptions, and models represent the structure's behavior faithfully. By identifying discrepancies, also possible to refine models to improve accuracy. Successful validation instills confidence in FEA results, guiding engineering decisions. This iterative refinement process enhances model accuracy, increase safety and performance of systems.

3.2.2.2 Modal Analysis

Modal analysis is used to study the dynamic characteristics of the structure, it is also used as an identification method in the field of engineering vibration [33]. Moreover, modal analysis provides better understanding into the dynamic behavior and structural integrity of conveyor idlers, helping in optimize their design, prevent resonance-related issues, predict failure modes, and ensure safe and reliable operation of the conveyor system. The modal analysis is the basis for any other dynamic analysis.

Mode frequencies obtained from modal analysis represent the natural vibration frequencies of the structure. These frequencies correspond to the structural modes, which are the characteristic patterns of vibration exhibited by the structure when subjected to dynamic loads or excitations. Each mode frequency indicates a specific mode shape, which describes how different parts of the structure move relative to each other during vibration [36]. These mode frequencies represent the natural frequencies at which the structure vibrates without any external forcing. They are determined by the mass, stiffness, and damping characteristics of the structure, and they provide crucial insights into its dynamic behavior and response to various environmental or operational conditions [36]. In structural dynamics analysis, engineers typically focus on identifying and analyzing a subset of the most critical mode frequencies that are relevant to the dynamic behavior and response of the structure under specific loading conditions. These critical frequencies are those associated with the lowest modes of vibration, which have the most significant influence on the overall structural response and performance [36].

Assuming that the studied system is characterized by undamped free vibration, since calculation shows that each particle of damping has limited effects on the frequencies and vibration model

of the roller [37]. Thus the governing equation for natural frequencies and mode shape is as follows:

$$[M] \times \{\ddot{x} + [K]x\} = 0 \tag{17}$$

In the formula (17), $[M]$ and $[K]$ are the total mass and stiffness matrix respectively, $\ddot{x}$, x are the acceleration and displacement vectors of the roller.

Also assume simple harmonic motion, i.e. represent *x* as follows:

$$\{x\} = \{x_0\} \sin(\omega t + \varphi), \tag{18}$$

where $\{x\}$ is modal, ω is the frequency of the corresponding mode, φ_0 is the initial phase.

$$\{[K] - \omega^2[M]\}\{x\} = \{0\} \tag{19}$$

Thus, $\{[K] - \omega^2 \times [M]\}$ reveal the natural frequencies, and $\{x\}$ represent the mode shapes of the studied system. Modal analysis is performed on the center roller.

The angular velocity w_{roller} is obtained by applying the following equation, by mean of linear velocity v_{belt}.

$$v_{belt} = w_{roller}\, r\,, \tag{20}$$

where r*:* center idler outer radius (m), linear velocity $v_{belt} = 2.9\ \mathrm{m/s}$

Assume no slippage, between belt and roller, linear velocity of the belt is transformed into angular velocity for the roller using the following equation

$$w_{roller} = \frac{v_{belt}}{r_{center-roller}} = 29.44\ \mathrm{rad/s}\,.$$

The frequency f_{roller} can be calculated from the angular velocity by the means of the following equation:

$$f_{roller} = \frac{w_{roller}}{2\pi} = 4.67\ \mathrm{Hz}\,. \tag{21}$$

The calculated frequency resultant from the velocity that is been transmitted to the roller thus it can be assumed that the frequency of the roller is the frequency of the belt. Thus the frequency of the roller is 4.67 Hz, also assuming that this frequency is the systems frequency.

Now applying modal analysis using Ansys Workbench software, the first 10 frequency modes, and mode shapes will be extracted from this analysis, since the structure is not that complicated, however, more complex structures with intricate geometries or irregular boundary conditions may exhibit a larger number of relevant modes.

a) Mode frequencies:

Table 3-5: First 10 mode frequencies extracted modal analysis (Stainless-steel).

Mode	Frequency (Hz)	Mode	Frequency (Hz)
1	290.63	6	743.72
2	292.98	7	755.35
3	334.74	8	780.66
4	607.73	9	785.55
5	609.57	10	950.19

The first ten mode frequencies are given in Table 3-5. Each mode corresponds to a specific natural frequency. The obtained modal frequencies indicate the natural modes of vibration of the structure. Lower frequencies correspond to lower-energy modes, while higher frequencies correspond to higher-energy modes. In addition, lower mode frequencies typically indicate larger-scale, global deformations of the structure. On the other hand, higher mode frequencies signify smaller-scale, localized vibrations. Upon examination of the mode frequencies derived from the modal analysis and their comparison with the calculated conveyor belt frequency of 5 Hz as determined by Equation (21), it is evident that the first mode frequency is 291 Hz, placing it outside the range of the belt frequency. This discrepancy indicates that resonance resulting from the belt frequency is unlikely to occur. Additionally, this analysis suggests that the belt speed can be elevated without concerns regarding resonance phenomena. Moreover, the extracted mode shapes corresponding to the mode frequencies are presented and explained in Appendix A.

3.3 Material Selection Criteria for roller Components

Upon concluding the analyses of the current structure using the existing material, the next step involves conducting an exhaustive study on material selection. This study carefully consider the design constraints, limitations, and environmental factors, ensuring informed decisions regarding the selection of materials that align with the desired specifications and operational requirements. Before starting the material selection procedure design requirements must be taken into consideration. As stated in Table 3-6 we start with the material selection for the roller shell.

Table 3-6: Design requirements for the roller shell.

Function	Roller shell
Constraints	High Strength, stiffness, wear resistance, corrosion resistance, temperature resistance. High fracture toughness, and hardness.
Objective	Minimize the weight, Maximize the overall effectiveness and efficiency
Free variable	Choice of material, Thickness of the shell

The main function of the roller shell is to meet the performance specifications for the conveyor belt, by supporting the belt an ensuring smooth functioning of the belt conveyor. The roller must have sufficient strength and stiffness to withstand the loads and stresses experienced during operation. Moreover, roller within the conveyor system must exhibit robust wear resistance to endure the abrasive effects of friction between the conveyor belt and conveyed material. Additionally, the selected material should demonstrate corrosion resistance against moisture and environmental factors. Furthermore, the roller shell material must withstand the system's operational temperatures without degradation and possess low friction characteristics to minimize energy losses and reduce wear on the conveyor belt.

The wear mechanism, elucidated in Figure 3–10, operates at a microscopic level, with specific requirements dictated by factors such as load magnitude, velocity, lubrication provisions, environmental conditions, and the coefficient of friction between interfacing surfaces. Abrasive wear, characterized by the gradual removal or displacement of material due to frictional interaction, is prominent between the conveyor belt and roller. This phenomenon is compounded by the adhesion of iron particles to the belt surface, as shown in Table 3-6 similarly, wear dynamics may manifest within bearings, including the clearance between bearing balls and the inner ring. To ensure operational longevity, the typical wear rate should not exceed 0.1 mm^3/m per 1000 hours of operation [19], thereby minimizing downtime and maintenance. Beyond wear resistance, material selection considerations encompass meeting a minimum hardness value of 60 HRC (Rockwell C scale) to withstand abrasive wear and maintain dimensional stability under applied loads. Additionally, materials should exhibit superior fracture toughness exceeding 20 joules at temperatures ranging from -30°C to 40°C. Temperature independence is crucial, ensuring sustained mechanical properties across a temperature range of -30°C to 40°C, with materials demonstrating low thermal expansion (<10 μm/m°C) being particularly desirable.

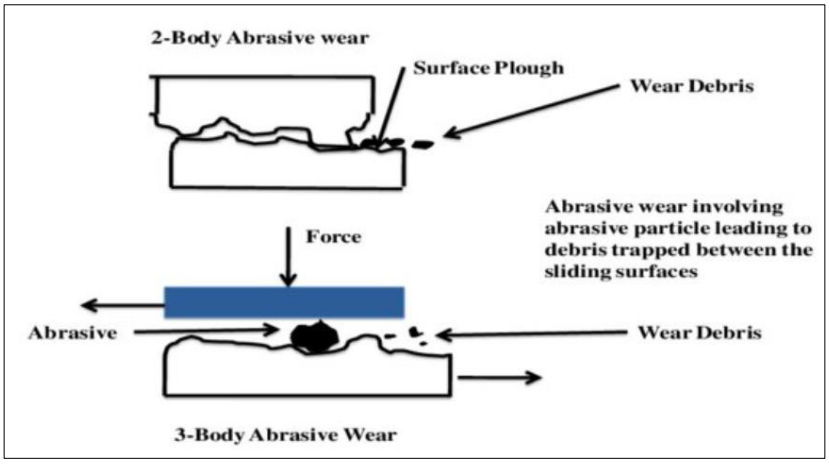

Figure 3–10: Schematics diagram of abrasive wear mechanism [38].

Taking all these constrains into consideration it is needed to keep the main objective which states minimizing the weight of the idler roller assembly, especially in critical maintenance areas where manual handling is required. There is freedom to choose materials and thicknesses for the roller shell, as long as the primary objective of weight reduction is met. The focus is on finding an optimal balance between structural integrity, durability, and decreased weight. This approach aims to improve operational efficiency and accessibility during maintenance tasks by making the roller assembly easier to handle.

As mentioned in Table 3-6 the objective is to minimize the weight of the conveyor idler thus the following objective function will be used according to Ashby's method to fulfill the requirements:

$$m = AL\rho = \pi rtL\rho\,, \tag{22}$$

where m: mass (kg), A: Area (m^2), L: length of roller (m), ρ: density (kg/m^3)

As shown in Figure 3–3 according to the load distribution acting on the central idler, the deflection is:

$$\delta_{shell} = \frac{5F_{Center}\,L^3}{384EI_{y-shell}}\,.$$

Moreover, the condition of thin walled tube is needed to be full filled.

$$\frac{r}{t} > 10,$$

where r is the tube outer radius, and t is the thickness. According to the data for the studied roller, the above condition is satisfied:

$$\frac{197}{6.2} = 32 > 10.$$

Thus according to [34] the moment of inertia $I_{y-shell}$ of thin walled tube can be replaced by:

$$I = \pi r^3 t\,.$$

Hence,

$$\delta_{shell} = \frac{F_{Center}\, L^3}{\frac{384}{5} EAtr}. \tag{23}$$

From (23) it follows that:

$$A = \frac{F_{Center}\, L^3}{\frac{384}{5} E\, \delta_{shell}\, r\, t}.$$

Inserting *A* into the objective function equation (22), knowing that the material index is function of material properties only we get:

$$m = L\rho \frac{F_{Center}\, L^3}{\frac{384}{5} E \delta_{shell} rt}.$$

Thus, the following material index should be maximized to get light stiff material

$$M_1 = \frac{E}{\rho}.$$

Moreover, selected material must be of high strength, to with stand the applied load:

$$\sigma_{yield} > \sigma_{applied}\,,$$

$$\sigma_{yield} > \frac{M_{max}\, y}{I_{y-shell}}, \tag{24}$$

$$M_{max} = \frac{F_{max}\, L}{8}. \tag{25}$$

Inserting (25) into (24), and solving for A reveals

$$A = \frac{\frac{FL}{8} y}{\sigma_{yield}\, r\, t}. \tag{26}$$

Inserting (26) into (22) gives that the following material index M_2 should be maximized in order to get strong light material

$$M_2 = \frac{\sigma_{yield}}{\rho}.$$

After calculating both M_1 and M_2 material indices corresponding to the conditions stated above, we apply calculated material indices to Granta EduPack software for material selection

along with the limits that where discussed previously regarding toughness, hardness, and thermal expansion. Charts were generated and are presented in Appendix C. However, the resultants materials from those charts are discussed and explained in Table 3-7. Results of material selection process are presented in Table 3-7 for comparison. As illustrated, CFRP, Titanium alloys shows priority, among all the other material in term of mechanical properties Young's modulus, yielding strength, hardness, and fracture toughness. However when it comes to the price, both materials shows higher prices than low alloy, steel, and stainless steel. Moreover, literature stated that mainly stainless steel, and alloy steels are commonly used in the manufacture of the conveyor roller.

Table 3-7: Comparison of the material selection results materials.

Material	**Mechanical Properties**	**Wear resistance**	**Hardness (HRC)**	**Toughness (J/m^2)**	**Approximate price ($per Kg)**
CFRP, epoxy matrix (isotropic)	High strength-to-weight ratio Excellent fatigue resistance Good corrosion resistance Modulus of elasticity: 70-140 GPa Tensile strength: 600-2000 MPa	Moderate	50-60	100-180	20 - 150
Low alloy steel	High tensile strength Good impact resistance Moderate corrosion resistance Modulus of elasticity: 190-210 GPa Tensile strength: 415-760 MPa	high	25-35	50-120	1.5 - 3
Stainless steel	Excellent corrosion resistance Good mechanical properties Modulus of elasticity: 190-200 GPa Tensile strength: 500-1000 MPa	Moderate to high	45-65	50-150	3 - 8
Titanium alloys	High strength-to-weight ratio Excellent corrosion resistance Good biocompatibility Modulus of elasticity: 100-120 GPa	Moderate	40-55	50-100	20 - 80

After conducting a comprehensive material selection study, it has been determined that stainless steel and low alloy steel, with some modifications involving the addition of a coating material to enhance structural durability, best fulfill the previously stated objectives. However, a review of the literature reveals that modern technology, as adopted by most manufacturers, favors composite materials such as CFRP and GFRP (Carbon and Glass Fiber Reinforced Polymers)

along with polymer materials like High-Density Polyethylene (HDPE) and Polyetheretherketone (PEEK), including its reinforced variant PEEK GF30 [39]. These materials offer favorable mechanical properties, light weight, as well as excellent wear and corrosion resistance. It is worth noting that both PEEK and PEEK GF30 are relatively more expensive compared to HDPE [39]. Therefore, HDPE emerges as a viable alternative material alongside stainless steel, warranting further analysis and study.

3.4 Optimization Techniques for Roller Shell Weight

Table 3-8 presents the physical and mechanical properties of the material chosen for analysis in optimizing the belt conveyor roller by minimizing the weight of the conveyor idler. It is evident that HDPE exhibits a lower density compared to stainless steel. Conversely, the modulus of elasticity of stainless steel surpasses that of HDPE, measuring at 1.08 GPa.

Table 3-8: Physical and mechanical properties of High-Density Polyethylene (HDPE) [40].

Physical and Mechanical Properties of High-Density Polyethylene (HDPE)	
Density	955 kg/m^3
Ultimate tensile strength	43 Mpa
Yield Tensile strength	28 MPa
Modulus of Elasticity	1.08 GPa
Hardness Rockwell C	52

Before proceeding with the analysis, a simple calculation for the minimum thickness of the center roller shell should be done to fulfill the condition of shell slope angle not exceeding 0.004 radian to insure that the bearing are functioning properly upon subjected load.

$$y_{shell} \leq 0.004$$

$$\frac{F_{center-distributed}\, L^3}{24 E I_{y-shell}} \leq 0.004\,,$$

$$\frac{4380 \times 0.95^3}{24 \times 1.08 \times 10^9 \times \frac{\pi}{4} \times (0.097^4 - r_{inner}^4)} \leq 0.004$$

Solving equation (11) get the minimum radius for avoiding this slope angle, we get $r_{inner} = 80.7\text{mm}$. Same argument is considered to insure that no failure due to yielding will occur, Referring to equation (24) it follows that:

$$\sigma_{yield} > \frac{My}{I_{y-shell}}$$

$$28 \times 10^6 > \frac{494 \times 0.097}{\frac{\pi}{4} \times (0.097^4 - r_{inner}^4)} \tag{27}$$

Solving equation (27) reveals $r_{inner} = 90\text{mm}$, which represent the minimum radius to prevent failure by yielding. To ensure compliance with both conditions, mainly maintaining a roller shell angular deflection less than 0.004 radians and preventing failure due to yielding, the smaller radius option is selected, resulting in $r_{inner} = 80.7\text{mm}$. However, for safety considerations, this value may be subject to adjustment. Moreover, since deflection is extremely small in case of stainless-steel, similarly to the stress distribution values it's not taken into consideration the thickness calculation, however the structural analysis to observe the maximum values upon new thickness is needed to be performed. Therefore, in the finalized design, the inner radius is set to be $r_{inner} = 75$ mm, this implies that the final shell thickness is 22 mm striking a compromise between deflection, stress levels, and the objective of minimizing the weight of the roller.

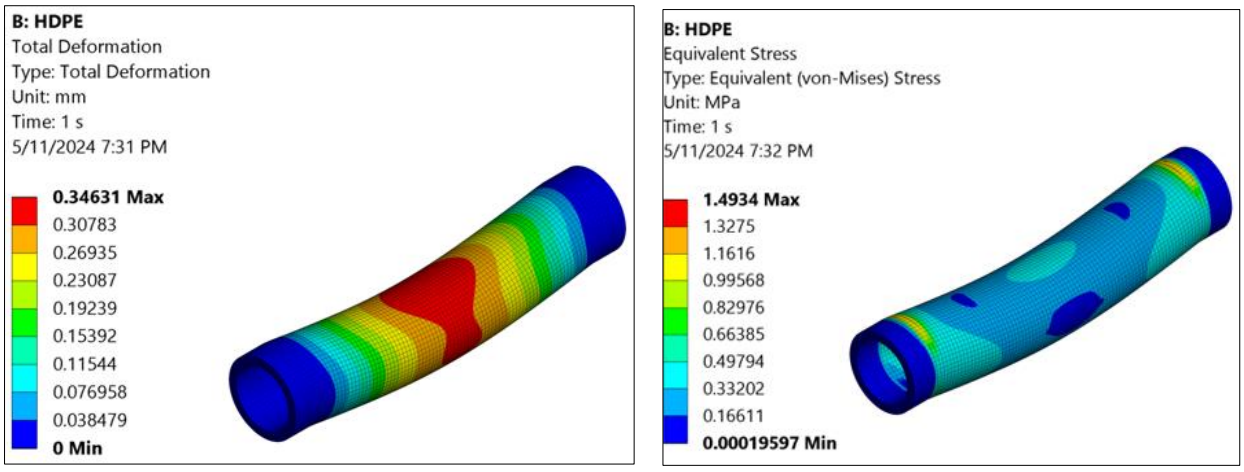

a) b)

Figure 3–11: a) Total deformation (mm), b) stress distribution (Mpa) of center roller shell.

Since only deflection slope was taken into consideration in thickness calculation, results of total deformation and stress levels show variation from the previous studied material for center roller shell with assigning the new material. The results are presented in Figure 3–11 the deformation

increases from 0.017 mm to it reaches 0.35 mm. However, the deformation values are still accepted since the slope deflection condition is satisfied. Similarly, the stress distribution shows a maximum value of almost 1.5 MPa in HDPE roller, showing maximum at the same section as previous analysis (bearing housing edge). This reveals that bearing housing hub edge is a transition section where the load is concentrated.

Properties	
Volume	1.1293e+007 mm³
Mass	14.343 kg
Centroid X	8.1394e-015 mm
Centroid Y	-2.1483e-002 mm
Centroid Z	475. mm

a)

Properties	
Volume	3.6956e+006 mm³
Mass	29.45 kg
Centroid X	-5.0284e-015 mm
Centroid Y	-2.3692e-002 mm
Centroid Z	475. mm

b)

Figure 3–12: Geometry properties of the shell rollers a) HDPE, and b) Stainless-steel.

However, still the values are below yielding strength which ensures that the structure is safe and will not fail under the applied loads. The formula for calculating mass reduction can be expressed as follows:

$$\%\ of\ Mass\ reduction = \frac{Mass_{initial} - Mass_{final}}{Mass_{initial}} \times 100 \quad (28)$$

According to the data presented in Figure 3–12 is follows that:

$$\%\ of\ Mass\ reduction = 50\%$$

Comparing the masses of the structure in both cases reveals a significant reduction of nearly 50%. This reduction translates into tangible benefits for maintenance cycles and repair time reduction. By implementing the new model with a mass of 14.5 kg compared to the existing model's nearly 29.5 kg, the objective of weight minimization is successfully achieved. This reduction in mass not only improves the overall efficiency and performance of the structure but also streamlines maintenance procedures and reduces repair time. With a lighter structure, maintenance tasks become more manageable, allowing for quicker inspections, repairs, and replacements. As a result, downtime is minimized, leading to enhanced operational uptime and productivity. Thus, the reduction in mass not only fulfills the weight optimization goal but also contributes to overall maintenance efficiency and operational effectiveness. Moreover, performed modal analysis for the new roller model ensure that the proposed HDPE material will not experience resonance phenomena. The results, illustrated in Table 3-9, reveal that the first 10 mode frequencies of the HDPE material range between 136 Hz and 350 Hz, well outside the belt's natural frequency of 5 Hz.

Table 3-9: First 10 mode frequencies modal analysis (High-Density Polyethylene HDPE).

Mode	Frequency (Hz)	Mode	Frequency (Hz)
1	135.99	6	286.11
2	137.07	7	289.15
3	190.15	8	308.3
4	197.07	9	345.12
5	237.76	10	346.88

Moreover, for understanding the effect of dynamic load on the structure's integrity, a dynamic analysis has been performed assuming that the structure is subjected to a harmonic periodic load of intensity 4380 N/m. The provided frequency response graph Figure 3–13 illustrates the dynamic behavior of roller in response to the harmonic applied load of intensity 4380 N/m. At its core, the graph shows the relationship between the natural frequencies (Hz) of the system and the resulting amplitude of its response (mm). Notably, a peak in the amplitude response is observed in the range of 125-150 Hz, indicative of resonance phenomena within the system, where the displacement amplitude amplifies till maximum reaching 5.7143 mm. This indicates that resonance occurs when the excitation frequency matches the natural frequency of the system which is exactly 140 Hz leading to amplified vibrations. On the other hand, beyond the resonant frequency, the amplitude gradually decreases, due to the fact that internal damping is presented within the system. Damping serves to dissipate energy and attenuate vibrations, ultimately stabilizing the system's response.

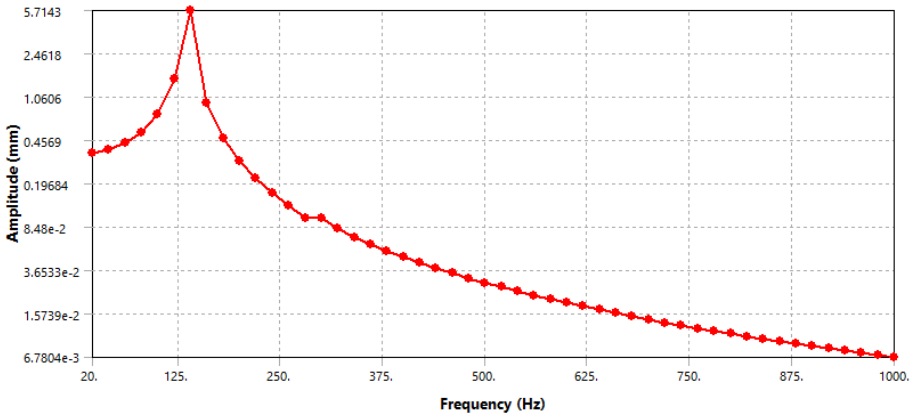

Figure 3–13: Frequency Response of HDPE roller under 4380 N harmonic load.

Therefore, it is obvious that the effect of dynamic load is more severe than that of static load if applied within a frequency that lays in the range of the natural frequency of the structure, since upon applying a static load of 4380 N/m the maximum deformation was around 0.4 mm,

however the same load was applied with a 140 Hz frequency shows directional deformation *y*-direction up to 18mm as shown in Figure 3–14.

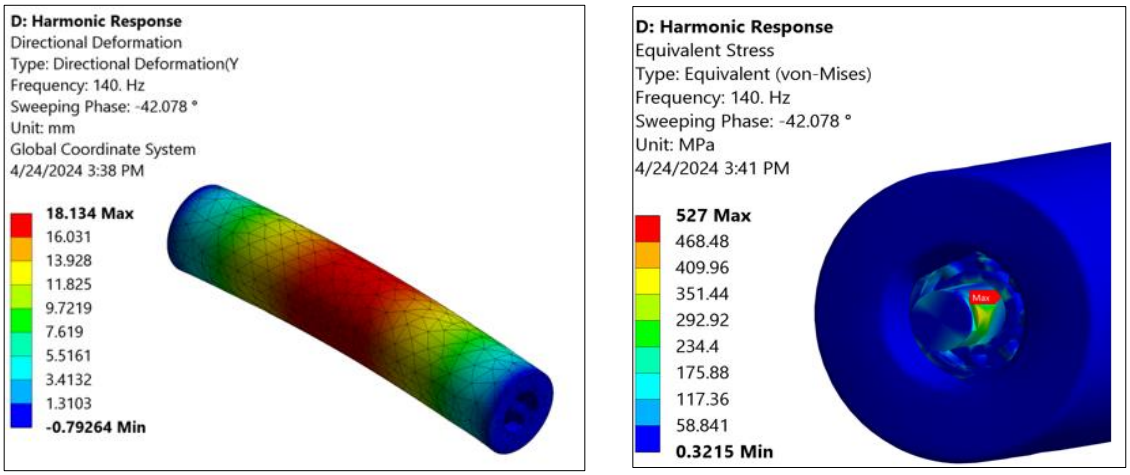

a) b)

Figure 3–14: a) Directional deformation (y-direction) (mm), b) Stress distribution (MPa).

Hence, to ensure the accuracy of the analysis it's important to acquire precise load profiles reflecting the actual structural behavior in real-world scenarios. However due to the lack of this information in the studied case, force profile was assumed to be harmonic of same intensity as the calculated static load.

3.5 Estimation of Bearing Lifespan and Maintenance Considerations

From the studies presented before one can conclude that bearing sizing is a fundamental aspect in the design of conveyor rollers, and it is important for ensuring efficient and reliable operation of conveyor systems in diverse industrial applications. Proper bearing sizing is essential for optimizing load-bearing capacity, minimizing friction, and maintaining smooth operation under varying loads and operating conditions [41]. By accurately sizing bearings to match specific application requirements, manufacturers can effectively mitigate the risk of premature bearing failure, extend bearing life, and reduce the need for frequent replacements, ultimately enhancing the overall performance and longevity of conveyor rollers [41]. As mentioned before behind shell failure, the most critical causes of idler replacement is bearing failure [24]. Figure 3–15 shows major type of bearing damage observed include increased gaps due to plastic deformations (42.3%), corrosive wear (30.7%), fretting corrosion (11.6%), fractures (8.2%), surface fatigue wear [41].

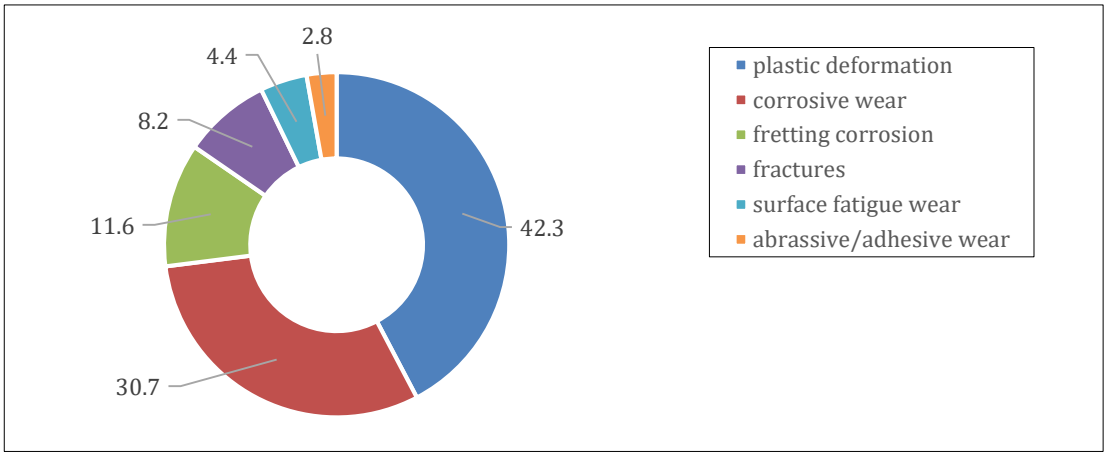

Figure 3–15: % of major bearing damage.

Accurate bearing sizing directly impacts bearing life estimation and can plays an important role in indicating premature bearing failure, causing of roller malfunctions and unplanned downtime in conveyor systems. Bearings that are undersized or inadequately matched to the application may experience excessive wear, fatigue, and overheating, leading to accelerated bearing degradation and reduced service life. Consequently, frequent bearing failures necessitate frequent roller replacements, resulting in increased maintenance requirements, downtime, and associated costs that can significantly affect the operational efficiency and productivity of conveyor systems. By prioritizing accurate bearing sizing and proactive maintenance practices, industries can optimize bearing life, minimize the frequency of roller failure and replacement, and ensure the long-term reliability and cost-effectiveness of their conveyor systems.

The studies offer a view into the factors leading to the replacement of idler rollers positioned at both the center and sides of conveyor systems. A common finding across these studies is the prevalence of bearing failure, often attributed to contamination, vibration, and friction-induced wear of the outer shell of the roller. Additionally, the accumulation of particles on the belt further exacerbates wear issues. The upcoming investigation is focused on an in-depth analysis of these pivotal aspects concerning idler rollers.

Estimation of the bearings lifespan in conveyor rollers enables organizations to adopt a proactive approach to maintenance, resulting in increased reliability, cost savings, and safety benefits for their operations. However, this estimation is not as simple as it looks like since there are many assumptions and factor that must be taken into account during the calculation process. First conditions to choose which method to be used in estimation of bearing life is the

lubrication condition. Figure 3–16 shows the lubrication regimes of an operating bearing, there are three primary regimes illustrates the interaction between the lubricant and bearing surfaces boundary, mixed, and full-film lubrication. Boundary lubrication involves a very thin film of lubricant, leading to intermittent metal-to-metal contact and high friction. Mixed lubrication combined aspects of both boundary and full-film regimes, with a thicker but incomplete lubricant film, occurring during transient conditions. Full-film lubrication, the ideal state, features a continuous, thick lubricant film that fully separates bearing surfaces, minimizing friction and wear for optimal performance. Each regime's occurrence depends on factors like load, speed, and lubricant properties. As stated in Figure 3–16 there are three-lubrication regimes each depends on the condition of viscosity ratio *k*:

$$k = \frac{\nu}{\nu_1}, \tag{29}$$

where:

ν *:* Actual viscosity of the lubricant at bearing operating temperature (mm²/s).

ν_1*:* Rated viscosity depends on the operating speed, and mean diameter of the bearing (mm²/s).

There are three main types of lubrication regimes according to viscosity ratio *k:*

- $k \leq 0.1$ $boundary\ lubrication.$
- $0.1 < k \leq 4$ $mixed\ lubrication.$
- $k > 4$ $hydrodynamic\ lubrication$ $(full - film\ lubrication)$.

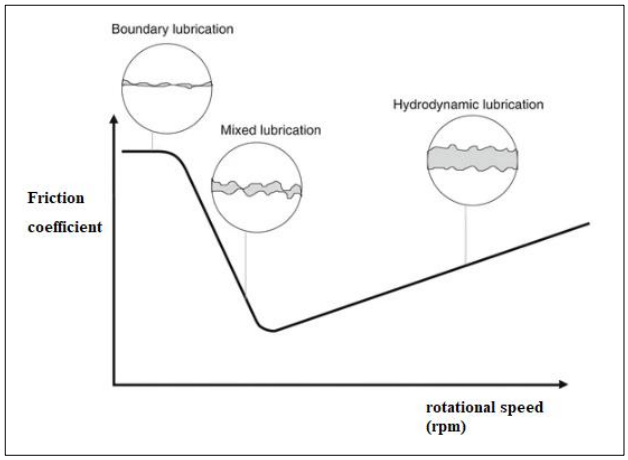

Figure 3–16: Types of lubrication regimes [42].

Thus, according to this condition the type of estimation can be done. If the bearing is operating in a full-film condition, constant loading, and appropriate speed, then bearing basic rating life is used to estimate the bearing lifespan. On the other hand if the bearing is operating in boundary

lubrication regime, low speed (below 10 rpm), sudden loading conditions, then static safety factor method is used to estimate bearing safety. Finally, if the bearing is operating in mixed lubrication condition with constant loading then basic rating life is used else if the bearing is in mixed lubrication condition, but subjected to sudden loadings and peak loads then static safety factor method is used. In this study the bearing used in the conveyor idler is 6308 SKF bearing, bearing data sheet is enclosed in Appendix C.

The lubrication condition (viscosity ratio *k*) is needed to be checked. It is assumed that used lubricant is SKF LGMT 2 (general purpose industrial and automotive NLGI 2 grease). According to the viscosity clarification (3448, Lubricant ISO VG100) from [43] the base viscosity is 110 mm²/s at 40 °C, and 11 mm²/s at 100 °C.

However, the operating temperature of the bearing is assumed to be 70 °C, then interpolating between these values the viscosity is 60.5 mm²/s.

Studying the center roller, it is assumed that there are no friction losses. Thus there is no slippage between roller and bearing. The mean diameter D_{mean} and the bearing operating roller speed n_{roller} are as follows

$$D_{mean} = \frac{D_{outer} + D_{inner}}{2} = 65mm\,.$$
$$n_{roller} = \frac{1000 \times 60 \times v_{belt}}{\pi \times D_{center-roller}}\,, \qquad (30)$$
$$n_{roller} = 285\text{rpm}\,.$$

where $D_{center-roller} = 194$ mm is the center roller diameter, $v_{belt} = 2.9$ m/s.

According to the data provided by SKF [29], the rated viscosity is 45 mm²/s.

Applying equation (29) we get:

$$k = \frac{60.5}{45} = 1.344\,.$$

The calculation of the viscosity ration reveals that the bearing is operating in mixed boundary lubrication condition, and since the study is on a center carrying idler, and upon conveying that there is no variations of the load, the load is assumed to be constant. Therefore, basic bearing rating life method is used to estimate the lifespan of the bearing.

Bearing basic rating life can be calculated according to ISO standards (ISO 281:2007), knowing that the provided equation is with 90% reliability which means that the bearing have 90% chance to reach or exceed L_{10}, and 10% to fail before reaching L_{10}. This formula represents the bearing life, the number of revolutions or the number of operating hours at a given speed that

the bearing is capable of enduring before the first sign of metal fatigue. L_{10} Formula only capable for (Rolling Contact Fatigue, RFC), but there are several factors that affect the bearing life:

- Lubrication conditions.
- Internal bearing clearance.
- External conditions.

For lubrication condition as we calculated before (mixed lubrications) supposing constant load then (Bearing Basic Rating Life) formula [19] ISO 281:2007 is as follows:

$$L_{10} = \left(\frac{C}{P}\right)^{p}, \tag{31}$$

where:

C: constant stationary load which a bearing can theoretically endure for a basic rating life of 1 million revolution (MR) [29].

P: dynamic equivalent load [29].

P: correlation constant: p = 3 for ball bearing , p= 3/10 for roller bearings. [19].

As calculated before, the load acting on the shaft is 4380 N calculated before for a shaft diameter of 40 mm as mentioned in Table 3-1. As a first step in calculating the bearing basic rating life, the minimum requested load F_{min}, according to the manufacture data sheet [29] is as follows:

$$F_{min} = K_r C\ , \tag{32}$$

where coefficient $K_r = 0.03$, and basic dynamic loading $C = 42.3$ kN are given by manufacturer data sheet [29].

The condition (32) needs to be satisfied, i.e. applied minimum load F_{min} should be at least greater or equal to the minimum requested load:

$$F_{min} = 0.03 \times 42.3 = 1.27 \text{ kN}. \tag{33}$$

Total applied load on the shaft due to materials weight, weight of the belt, and roller is F_{tot} =4.38 kN. Thus, each bearing will experience $\frac{F_{tot}}{2}$ =2.19 kN. Since $\frac{F_{tot}}{2} > F_{min}$, the requirement (33) is fulfilled.

There is another condition to be satisfied, namely, the bearing speed n_b should be less than so-called limiting speed $n_{lim} = 17000$ rpm, and reference speed $n_{ref} = 11000$ rpm given by manufacturer [29].

$$n_b < n_{lim}, \qquad n_b < n_{ref} \tag{34}$$

Since $n_b = 285$ rpm, thus condition (34) is satisfied.

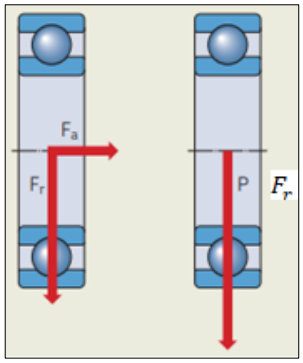

Figure 3–17: Free body diagram a) combined axial, radial loading, b) pure radial loading [29].

Calculating the ddynamic equivalent load *P*, the following equation is used [29]:

$$P = XF_r + YF_A \, . \tag{35}$$

where *X*, and *Y* are constants corresponding to radial, and axial load share factors values are mentioned in bearing data sheet [29]. F_r, and F_A represents the loads in radial and axial direction respectively.

For deep groove ball bearings it appears that *P*=*Fr* as long as $\frac{Fa}{Fr} < e$ where *Fa* being the axial load and *Fr* the radial load. However if $\frac{Fa}{Fr} > e$ then the equivalent bearing load *P* is calculated using equation (35).

In the studied case as mentioned before studying the center idler, and assuming that the force in distributed uniformly in radial direction, and there is no load acting in axial direction. Thus, YF_A is zero and dynamic equivalent load *P* is reduced to the following:

$$P = F_r = 2190N.$$

However, in the case of axial load wing roller case. *X*, *Y* can be derived from calculation factors for deep groove ball bearing K_{bb} according to the ratio refer to SKF bearing data tables [29]:

$$K_{BB} = \frac{f_0 F_A}{C_0}, \tag{36}$$

where f_0 is the calculation factor, C_0basic static load rating [29], and we get the values of *X*, *Y*, from table of Calculation factors [29]. However, in this case there is no need for this procedure since it is assumed that only radial force is applied.

Plugging the calculated values *C*=42.3 kN and *P*=2.19 kN into equation (31):

$$L_{10} = \left(\frac{42.3}{2.19}\right)^3 = 7206 \, MR \, .$$

where (MR) is million revolution.

Transferring L_{10} to working hours L_{10H} according to [29], give the following

$$L_{10H} = \frac{10^6}{60n} L_{10} = 421{,}386 \text{ hours} \tag{37}$$

Thus the working hours of the chosen bearing is $421{,}386$ hours which is quit number of working hours however, it's important to keep in mind that the calculations is done for the Rolling contact fatigue (RCF) with an assumption of ideal operating conditions assuming no clean conditions, no excessive load, well lubrication condition, and suitable operation speed of 3m/s. Neglecting the external conditions such as dust and water presence which plays a crucial role upon operation.

Comparing the calculated life hours with the recommended life of bearing which is (40,000-50,000) hours for 24 hours continuous working machines in our case conveyor idler [29], we get $421{,}386 \text{ hours} > 50{,}000 \text{ hours}$ .This indicates that the bearing is operating under less severe conditions than expected. That could be due to factors such as lower loads, slower speeds, or better lubrication than initially assumed. Although the above calculation indicates that the bearings used in this application in the assumed loads, speed, and lubrication conditions, but there are other factors that affect the operation of the bearing such as environmental conditions, moisture, dust, and dribs contamination. A summary for the above calculation is presented in Appendix B.

3.6 Contamination Problem Solution

After the lifespan estimation of SKF 6308 bearing, that is used in the most idlers available in the market, analysis indicates that the lifespan of the bearing is much greater than the recommended bearing life provided by SKF, however going to the practical case it shows that the bearing are still failing due to other reasons such as environmental conditions, contaminants accumulation on the bearing raceway, which incase increases friction, wear, and the risk of premature failure. Thus, the idea of using a shield bearing as shown in Figure 3–18 comes out to provide additional protection for the bearing, moreover preventing debris from accumulating in the bearing raceway.

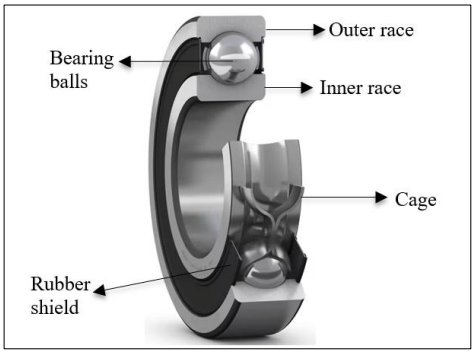

Figure 3–18: Rubber shield bearing cross-section [43].

In the application of conveyor systems, the choice of bearings plays an important role in ensuring efficient and reliable operation. Table 3-10 provides a detailed comparison between traditional and rubber-shielded bearings of the same series, highlighting the advantages of rubber shielded bearings, and what might be challenging. Rubber shielded bearings offer an effective barrier against contaminants such as dust, dirt, and moisture, reducing the risk of contamination accumulation within the bearing assembly and thereby extending the bearing life and enhancing overall reliability [43]. Furthermore, the incorporation of rubber shields contributes to noise and vibration reduction, resulting in a quieter and smoother operation of the conveyor system. However, it's important to note that this type of bearing may experience slightly higher friction due to the presence of the rubber shield between the inner and outer races of the bearing. Additionally, rubber shielded bearings may incur a slightly higher initial cost compared to traditional bearings due to the added expense of the rubber seals or shields [43]. Despite these challenges, the extended service life and reduced maintenance requirements offered by rubber shielded bearings often justify the investment, leading to long-term cost savings.

Table 3-10: Comparison between normal and rubber shielded bearings.

Aspect	**6308 Bearing**	**6308 Rubber Shielded Bearing**
Design	Open design no shields	Rubber seals or shields on both sides
Contamination Protection	Minimal contaminants protection.	Provides an effective barrier against dust, dirt, and moisture ingress
Lubrication	Requires regular lubrication	Retains lubricant more effectively due to rubber shields
Friction	Generally lower friction	Slightly higher friction due to rubber shields
Noise	Generate more noise	Rubber shields help dampen vibrations, resulting in quieter operation
Maintenance	Requires periodic cleaning	Shields may require occasional cleaning, but maintenance intervals are generally longer
Cost	Lower initial cost	Slightly higher initial cost due to rubber seals or shields

In bearing systems, shield bearings serve a crucial role in protecting the internal components from contaminants and ensuring smooth operation [43]. These bearings can be sealed on either sides or only one side, offering different levels of protection depending on the application requirements. Sealed bearings provide a barrier against dust, dirt, and moisture ingress, minimizing the risk of contamination and extending the bearing life [43]. They can be further classified into contact and non-contact seals, where contact seals create a physical barrier

between the bearing and the environment, while non-contact seals rely on clearance gaps to prevent contamination ingress. Each type of seal has its advantages and limitations, and the choice depends on factors such as operating conditions, maintenance requirements, and desired level of protection [43]. Although studies demonstrate the benefits of shielded bearings, but various factors can influence their performance. Thus, experiments comparing them with non-shielded bearings are essential. These experiments should analyze contamination protection, lubrication, friction, noise reduction, maintenance, and cost-effectiveness. Conducting such experiments helps in understanding the characteristics and performance of shield bearings, and provides valuable insights to optimize bearing selection for conveyor idler applications.

Chapter 4: Discussion & Conclusion

In conclusion, identifying failure causes and considering the position of each replaced idler is an essential procedure that a maintenance teams would have for crafting targeted solutions for the failures are facing in the facility, streamline their efforts, leading to more effective and timely solutions, reduced downtime, and improved system reliability. The comprehensive analysis conducted on the conveyor idler rollers within the LKAB facility in Narvik has offered understanding into their static, dynamic behavior, failure modes, and potential avenues for improvement. Through a multifaceted approach covering static, modal, failure mode and effects analysis (FMEA), and material selection, this thesis have identified critical areas of concern and proposed targeted solutions to enhance the reliability and lifespan of the conveyor rollers.

The static analysis results have provided data on the structural integrity and load-bearing capacity of the idler rollers, guiding our material selection approach. By integrating these findings into the material selection process, we have identified lightweight yet robust materials such as advanced engineering plastics such as High-Density Polyethylene (HDPE), Polyetheretherketone (PEEK), and composite materials such as CFRP and GFRP (Carbon and Glass Fiber Reinforced Polymers), which offer a balance of strength, stiffness, and wear resistance. Performed FEA shows that the stress distribution among the center idler decreases from maximum of 4 MPa in the existing roller, till it reaches 1.4 MPa in the proposed material (HDPE). Moreover, shell deflection of central idler was 0.34 mm for the proposed material (HDPE), with a shell thickness of 22 mm which lays on the acceptable range of deflection, showing a mass reduction of 50%, where the shell mass decreases from 29.5kg stainless-steel to 14.5 kg for HDPE.

Moreover, modal analysis conducted in this study has provided some understanding into the vibrational behavior of the idler rollers, informing our design considerations for conveyor systems. By identifying mode shapes corresponding to specific natural frequencies we gained a deeper understanding of the dynamic characteristics of the idler rollers. Additionally, the modal analysis revealed that the first ten mode frequencies of both the existing and proposed idlers fall outside the critical frequency range of the belt, which is 5 Hz and the range of 290-950 Hz for the stainless-steel and 136-350 Hz for HDPE, respectively. This indicates that neither models is subjected to resonance phenomena, reducing concerns regarding potential

resonance-induced vibration. Consequently, this finding allows for greater flexibility in adjusting the velocity of the belt, as the risk of resonance-induced vibration is minimized. Overall, the modal analysis serves as a crucial tool in optimizing the design and operation of conveyor systems, ensuring reliable performance and minimizing the risk of vibration-related issues.

Additionally, the in-depth study of bearing lifespan conducted in this research has yielded notable results regarding the divergence between theoretical calculations and practical outcomes. It has been discovered that the used bearings are seemingly overdesigned, with a calculated lifespan exceeding the manufacturer's provided value by approximately 350,000 working hours, far surpassing the specified hours by manufacturer which is 50,000 hours [29]. Despite this obvious excess in calculated lifespan, the bearings are still experience failures in real-world application scenarios. This deviation emphasizes the critical importance of considering operational conditions in the bearing sizing and selection process. While theoretical calculations may indicate sufficient bearing capacity, practical operating conditions can introduce unpredicted challenges and stresses that affect bearing performance. Therefore, it is imperative to conduct further experiments that take into account the specific operating conditions and environmental factors encountered in real-world applications. By incorporating such considerations into the bearing selection procedure, to ensure more accurate and reliable bearing performance, and ultimately enhancing the longevity of the idler in the facility. In summary, continuous refinement suggestions are presented in the coming chapter aiming to boost system performance and longevity, enhancing mining operation productivity for LKAB mining conditions.

Chapter 5: Further Work

While this thesis explores various aspects of conveyor belt rollers, starting from static and dynamic structural analysis, bearing failure assessment and lifespan calculations, and finally material selection for roller shells, there remain areas for exploration, future studies can capitalize to enhance existing solutions, investigate innovative technologies, and formulate comprehensive strategies aimed at enhancing the performance, durability, and sustainability of conveyor rollers.

- **Idler Monitoring Procedures**

At LKAB Narvik facility, a targeted approach to enhance idler replacement procedures is proposed. This involves implementing a standardized inspection protocol to ensure thorough assessments and detailed documentation of replacement causes and idler positions. This helps in investigation root cause for idler failure, facilitating the process of generating targeted solutions for the failure causes.

- **Dynamic Analysis and Loading Simulation**

Modal analysis provides basis information for the dynamic behaviour of conveyor rollers, aiding in the identification and mitigation of resonance phenomena. By examining natural frequencies and mode shapes, it is possible to can adjust design parameters for optimal performance. Further studies can explore the effects of dynamic loading conditions, simulating scenarios encountered in the LKAB Narvik facility. Understanding these dynamics informs design modifications to minimize vibration and enhance performance under real-world conditions.

- **Shaft-less / Hollow Shaft Designs**

One promising study is of shaft-less rollers, which eliminate the traditional shaft design, offering advantages like reduced costs, simplified maintenance, and increased conveyor flexibility. Another area of interest is the exploration of hollow shafts in roller design, which can achieve weight reduction while maintaining strength and stiffness. Hollow shafts have the potential to enhance structural efficiency by optimizing material distribution along the roller axis.

- **Bearing, Solid / Dry Lubricant Studies**

A comprehensive study that emphasizes the importance of considering environmental factors in bearing selection and operational conditions can be performed, along with an experimental investigations at LKAB Narvik facility focus on assessing the static safety factor of bearings and optimizing design. Additionally, further analysis and experiments are proposed to validate the effectiveness of using "Rubber Shield Bearings" to prevent contamination accumulation. Moreover, the analysis of lubrication conditions offers another approach for addressing contamination concerns, by exploring alternative lubrication options such as solid or dry lubricants could enhance lubrication performance while mitigating contamination risks in conveyor systems. Further research in this area promises data into optimizing conveyor idler reliability.

- **Bearing housing (Damped material Coating)**

The operation of a rotating element at critical speeds frequently causes a high level of mechanical vibration, noise and excessive wear. An important objective regarding rotating elements is either to eliminate major resonances or to avoid operating the equipment at speeds which could induce them. All shaft/bearing systems have a large number of frequencies at which they tend to vibrate. These are the so-called eigen frequencies or natural frequencies. They are determined by the mass and stiffness distribution of the shaft as well as the location and stiffness of the supporting bearings. Sometimes the compliance of the housing also has a significant influence [44]. The vibrating system of the idler bearing can be modeled according to Figure 5–1–1, and studied explicitly, by performing modal, and dynamic analysis of the rolling elements of the idler.

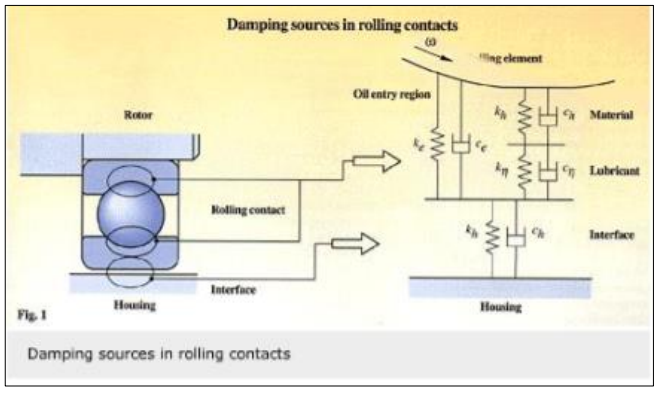

Figure 5–1–1: Damping source in rolling element [44].

The idea of applying damping coatings to bearing housings may help reducing vibrations and minimizing noise levels in rotating machinery. These coatings are typically viscoelastic in nature, meaning they possess both viscous and elastic properties. As a result, they can absorb and dissipate mechanical energy generated by vibrations, thereby reducing the transmission of vibrations to the surrounding structure. By reducing vibration levels, these coatings help minimize wear and fatigue on bearing components, extending their service life and reducing the likelihood of premature failure. However, it's important to note that the selection and application of coatings for bearing housings depend on various factors, including the specific operating conditions, environmental factors, material compatibility, and cost considerations. Therefore, while damping coatings may not be as widely used as other types of coatings, they can still offer valuable benefits in certain applications where vibration damping is a priority. Knowing that most of the damping coating materials are viscoelastic, the viscoelastic properties of the coating allow it to conform to irregularities in the sealing surfaces, creating a more effective and reliable seal against contaminants .Therefore, in such a study, it is promising examine two critical aspects contributing to conveyor idler (vibration and dribs contamination) both of which are recognized as significant factors leading to bearing failure.

- **Thermal Analysis (HDPE Roller)**

The selection of HDPE as the roller shell material offers numerous advantages, including corrosion resistance, low friction, lightweight design, impact resistance, cost-effectiveness, ease of fabrication, and environmental sustainability. These qualities make HDPE an ideal choice for conveyor rollers. However, while HDPE excels in these areas, its thermal properties are inferior to those of aluminum, steel, and stainless steel, which have higher thermal conductivity, lower coefficients of thermal expansion, higher melting temperatures, and greater thermal stability. Consequently, thermal analysis is imperative to assess the thermal performance of the proposed material under operating conditions.

References

[1] B. Janse van Rensburg, “The development of a light weight composite conveyor belt idler roller,” 2013.

[2] Nenad Zrnić, et al. “History of Belt Conveyors until the End of the 19th Century.” History of Mechanism and Machine Sciense, 1 Jan. 2022, pp. 210–223, [Online] Available: https://doi.org/10.1007/978-3-030-98499-1_18.

[3] P. M. McGuire, Conveyors: application, selection, and integration. CRC Press, 2009.

[4] Business Sweden, Mining for generations, [Online] Available: http://www.miningforgenerations.com/learn-more-about-swedens-mining-industry

[5] Teams, Interviewee, *LKAB- Narvik.* [Interview]. 05- February- 2024.

[6] LKAB-Briefing, Thailand’s Office of Industrial Affairs, Vienna,[Online] Available: https://thaiindustrialoffice.files.wordpress.com/2016/01/lkab.pdf.

[7] CEMA, Belt Conveyors for Bulk Materials Calculations by CEMA 5th Edition, CEMA.

[8] RULMECA, Rucmela Catalog_Bulk_Handling_EN.pdf, Italy: RULMECA.

[9] R. Nascimento, R. Carvalho, S. Delabrida, A. Bianchi, R. A. R. Oliveira, and L. G. U. Garcia, “An integrated inspection system for belt conveyor rollers,” in Proc. 19th Int. Conf. Enterprise Inf. Sys.(ICEIS), 2017, vol. 2, pp. 190–200.

[10] SKE Industries for Bulk Material handling, Troughed Idlers for Belt Conveyor, [Online] Available: www.skecon.com/accessories/conveyor-idlers/troughing-idlers.html

[11] S. Industries, “Conveyor-Idlers-literature.pdf,” [Online] Available: https://superior.widen.net/s/fczjgnnjkd/conveyor-idlers-literature

[12] Ocean Rubber Factory LLC, “Conveyor-Idlers-ORF Rollers”, [Online] Available: https://conveyor.orf.ae/orf-rollers/

[13] B. Janse van Rensburg, “The development of a light weight composite conveyor belt idler roller,” 2013.

[14] Rulmeca, ”Heavy Duty Conveyor Rollers - PSV | Rulmeca,” [Online] Available: https://www.rulmeca.com/en/products_bulk/catalogue/1/belt_conveyors/1/belt_conveyor_rollers/4/heavy_duty_conveyor_rollers_psv

[15] S. Industries, “Steel Idlers,” Superior Industries, [Online] Available: https://superior-ind.com/products/conveying-parts/idlers-return/steel-standard-40-series-idler-roller/

[16] R. Roller Company, “RKM Heavy Duty Lightweight Composite Roller,” [Online] Available:https://rkmrollers.com.au/products/rollers/rkm-heavy-duty-lightweight-composite-roller

[17] A. Frittella and G. Cohen, “Conveyor idler standards,” Melco Mining, 2008.

[18] CEMA, “CEMASTORE – Publications from the Conveyor Equipment Manufacturers Association (CEMA),” [Online] Available: https://cemastore.com/product/cema-belt-conveyors-for-bulk-materials-7th-ed-eng-book-pdf/. https://www.cemastore.com

[19] I. S. Association , “ISO - 53.040.20 - Components for conveyors,” [Online] Available: https://www.iso.org/ics/53.040.20/x/

[20] A. Frittella and S. Curry, “Conveyor idlers-SANS 1313 and selection procedures,” in Proc. Beltcon 15 Conf., 2009, pp. 1–14.

[21] B. S. Institution, “British Standards Institution - Project,” [Online] Available: https://standardsdevelopment.bsigroup.com/projects/2022-01054#/section

[22] J. I. Standards Committee, “JISC-Japanese Industrial Standards Committee,” [Online] Available: https://www.jisc.go.jp/eng/

[23] I. E. Loureiro et al., “Analyzing conveyor idler replacement causes: Insights from idler type and position,” in ICBMH2023: 14th International Conference on Bulk Materials Storage, Handling and Transportation: 14th International Conference on Bulk Materials Storage, Handling and Transportation, 2023, pp. 517–522.

[24] X. Liu, “Prediction of belt conveyor idler performance,” TRAIL Research School, 2016.

[25] X. Liu, Y. Pang, G. Lodewijks, and D. He, “Experimental research on condition monitoring of belt conveyor idlers,” Measurement, vol. 127, pp. 277–282, 2018. rollers. In Proc. 19th Int. Conf. Enterprise Inf. Sys.(ICEIS) (Vol. 2, pp. 190-200).

[26] S. Hötte, S. von Daake, L. Schulz, L. Overmeyer, and T. Wennekamp, “Science-The Way to DIN 22123—Indentation Rolling Resistance of Conveyor Belts,” Bulk Solids Handling, vol. 32, no. 6, p. 48, 2012.

[27] A. Pytlik and K. Trela, “Research on tightness loss of belt conveyor’s idlers and its impact on the temperature increase of the bearing assemblies,” Journal of Sustainable Mining, vol. 15, no. 2, pp. 57–65, 2016.

[28] R. Król and W. Kisielewski, “Research of loading carrying idlers used in belt conveyor–practical applications,” Diagnostyka, vol. 15, no. 1, pp. 67–73, 2014.

[29] “SKF,” [Online] Available: https://www.skf.com/id/products/rolling-bearings/principles-of-rolling-bearing-selection/bearing-selection-process/bearing-size.

[30] A. Mehta and G. Barker, “The dynamics of sand,” Reports on Progress in Physics, vol. 57, no. 4, p. 383, 1994.

[31] L. Hrabovskỳ, “Cross-Sectional Area Of The Belt Conveyor With A Three-Idler Set,” Perner’s Contacts, vol. 6, no. 2, pp. 62–67, 2011.

[32] LKAB, “TR010,” LKAB, Narvik, 2024.

[33] Rao, S.S. Mechanical Vibration. 5th Edition, Pearson Education, Inc., Upper Saddle River, 603-606. (2006)

[34] Hibbeler, R. C. Structural analysis. Boston :Prentice Hall, (2015)

[35] G. Tooker, “The economics of idler load rating and spacing,” Bulk Solids Handl.;(Germany, Federal Republic of), vol. 8, no. 6, 1988.

[36] S. Timoshenko, D. H. (Donovan H. Young, and W. Weaver, Vibration problems in engineering, 4th ed. New York: Wiley, 1974.

[37] Q. Wang, W. Xiong, and X. Wang, “Modal Analysis of Belt Conveyor Roller,” in 2015 International Conference on Intelligent Systems Research and Mechatronics Engineering, 2015, pp. 1661–1664.

[38] Z. Yusoff and S. B. Jamaludin, “Tribology and development of wear theory: Review and discussion,” 2011.

[39] PEEK plastic material | Ensinger,” [Online] Available: https://www.ensingerplastics.com/en/thermoplastic-materials/peek-plastic

[40] MatWeb, “Online Materials Information Resource - MatWeb,” [Online] Available: https://www.matweb.com/

[41] M. Vasić, B. Stojanović, and M. Blagojević, “Failure analysis of idler roller bearings in belt conveyors,” Engineering Failure Analysis, vol. 117, p. 104898, 2020.

[42] Q. J. Wang and Y.-W. Chung, *Encyclopaedia of tribology*. Springer US, 2013.

[43] SKF, “General purpose industrial and automotive bearing grease,” [Online] Available: https://www.skf.com/id/productinfo/productid-LGMT%202%2F180

[44] SKf, “Damping in a rolling bearing arrangement - Evolution,” DAMPING IN A ROLLING BEARING ARRANGEMENT, Feb. 15, 1996. [Online] Available: https://evolution.skf.com/damping-in-a-rolling-bearing-arrangement/

[45] ANSYS, “Modal Analysis | Ansys Innovation Courses,” Innovation Space. [Online] Available: https://innovationspace.ansys.com/product/modal-analysis/

[46] SKF, “Bearing Calculations,” [Online] Available: https://www.skf.com/id.

Appendix A

A.1 Analysis Set-up

Static Structural Analysis (Shaft and Roller):

Experimental Set-up for the center roller shaft static analysis, after importing the geometry that have be drawn before in Solid works to Ansys Workbench software start with assigning the material type for the shaft that was chosen to be Stainless steel. Proceeding to meshing stage after assigning the shaft material set the mesh type and size:

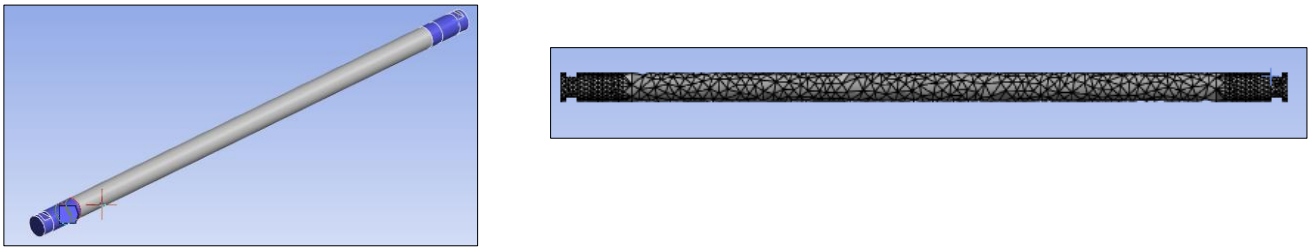

Figure A–1: Shaft meshing

Quadratic mesh type was used in meshing the shaft element however, in the bearing place it is a critical area thus the mesh size was finer 5mm, however, the rest of the shaft the mesh size was 10mm.

After meshing the element shown in Figure A–1we apply the boundary conditions as shown in Figure A–2.

Upon setting the analysis, shaft is assumed to be fixed ended at both sides thus there exists reactions forces and moments acting in all directions (x, y, z), insuring that the shaft will remain fixed. Below is a 2D figure and analysis set up showing the reactions on the shaft, for reactions visualization.

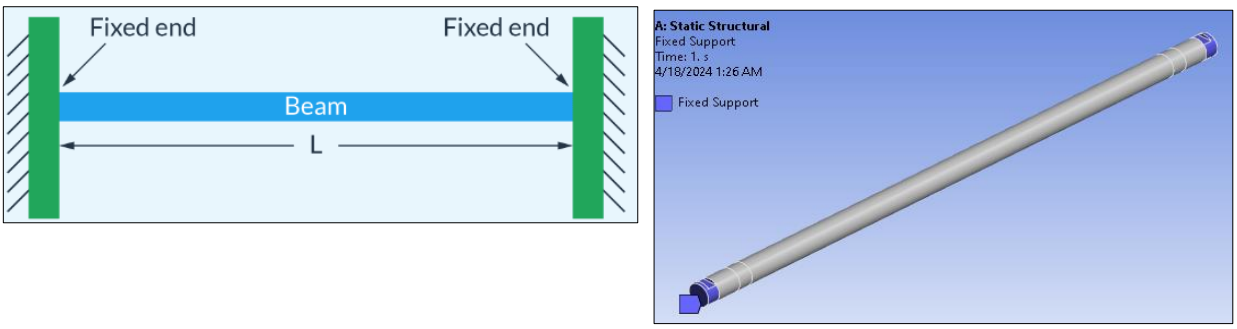

Figure A–2: Shaft support

Apply the loads and run the analysis to get the deformation and the stress distribution. Note that the assuming that the distributed load is applied at the bearing place and the distributed load is divided by half. Moreover the weight of the shaft was also assumed during the analysis.

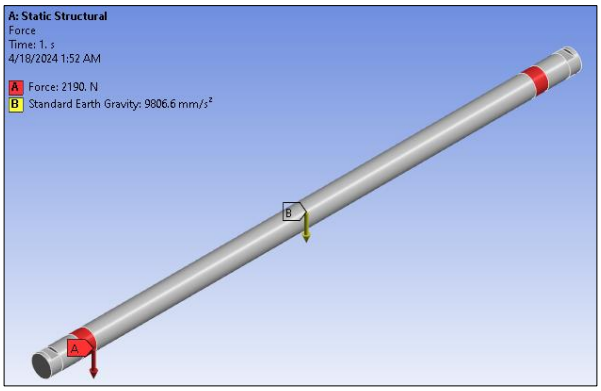

Figure A–3: Shaft loading conditions.

Roller Shell Analysis Set-up Ansys Workbench:

Similar, steps was done for the roller analysis from material selection to meshing the element. However, for the roller shell it is assumed to be fixed supported in (x, y, z) direction, While, it is only allowed to rotate along its axis (x-axis).

For the loading conditions it's assumed that the load excreted by the material to be uniformly distributed over the upper face of the roller with an intensity of 4610N/m. Moreover, the own weight of the roller was taken into consideration upon performing the simulation

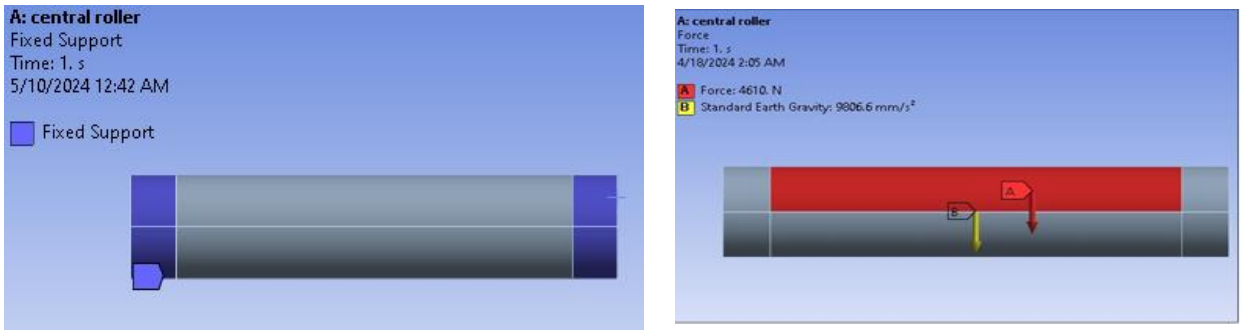

Figure A–4: Roller boundary conditions

Roller Shell Analysis Set-up Ansys Mechanical APDL:

For this simulation, first we assign the type of analysis as structural analysis, then element type was chosen to be beam element 188, after that the beam section was defined as a hollow cylinder, after that assign material properties and model the geometry.

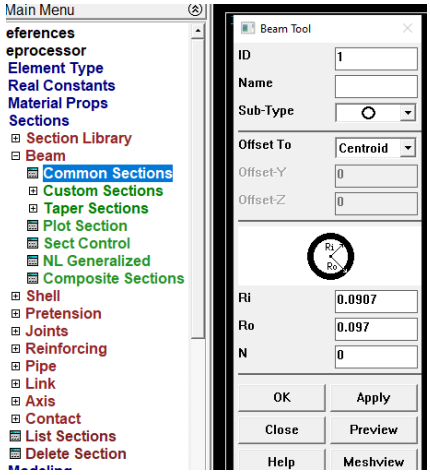

Figure A–5: Defining section Ansys Apdl

Mesh element size was chosen to by 0.025 due to software limitations (student version), as shown below.

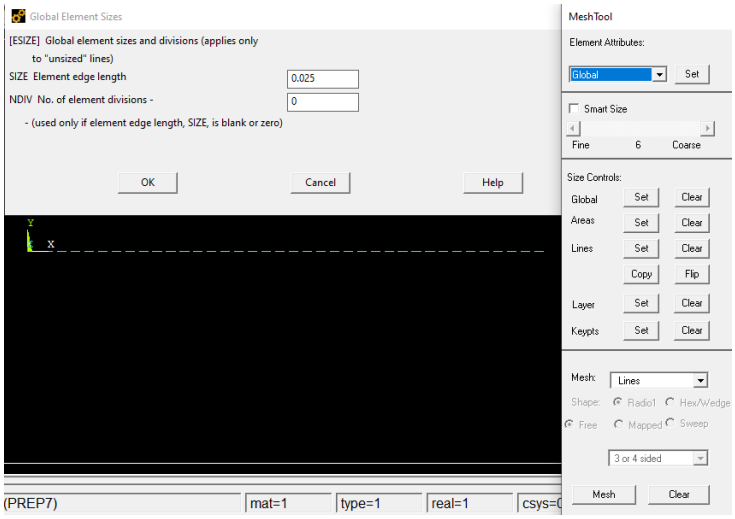

Figure A–6: Roller meshing details Ansys Apdl

After meshing the geometry, structural constrains was applied along with the loads as shown below. Upon setting up the analysis, the analysis is now ready for solution.

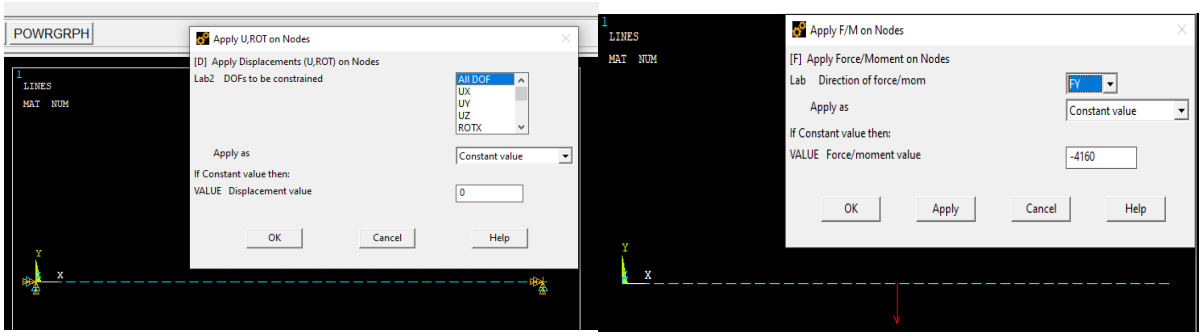

Figure A–7: Roller boundary conditions details Ansys Apdl

Modal Analysis Set-up and Mode shapes:

Modal analysis focuses on stiffness and mass-dependent factors, so only the supports will be applied for the structure. Moreover, due to software limitations on meshing elements, a default meshing option was chosen:

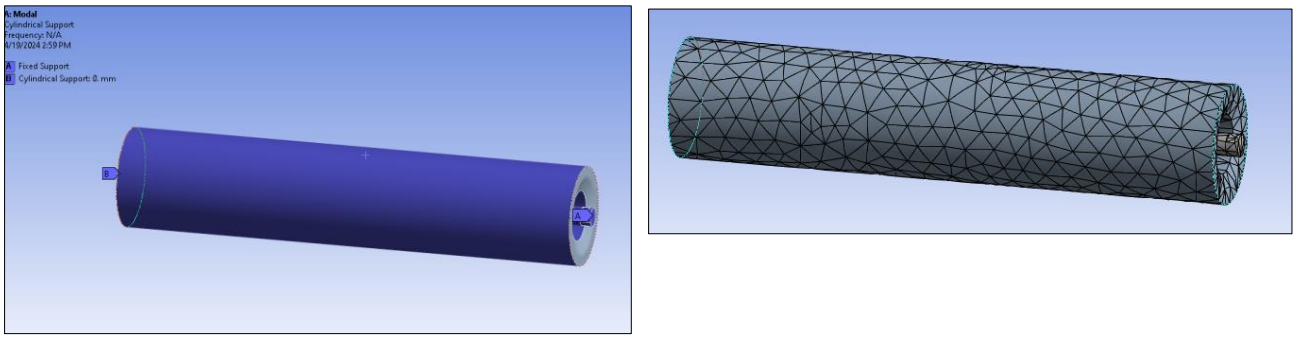

Figure A–8: Roller Support and meshing conditions.

After running the analysis, mode frequencies were extracted and discussed in Table 3-5, in addition to the mode shapes that are presented in Table A-1. Mode shapes represent the vibrational patterns or shapes assumed by a structure in response to an excitation or external load, these modes are characterized by their displacement patterns, and number of mode shapes corresponds to the number of degree of freedoms of the system. These mode shapes can be bending, torsional, axial, shear, and combined modes, and each of these modes is associated to a natural frequency, which represent the frequency at which the structure vibrates most efficiently in that particular mode in that particular shape. As previously discussed, the modal analysis reveals distinct mode shapes, each associated with a specific natural frequency. Table A-1 illustrates the amplified deformations of mode shapes alongside their corresponding natural frequencies. Note that the numbers presented in the table below corresponds to the mode frequencies presented in Table 3-5 respectively.

Table A-1: Mode shapes corresponding to mode frequencies for center shaft and roller.

1 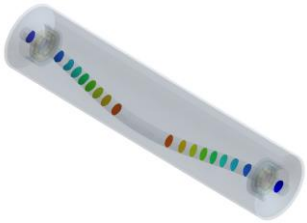	**2** 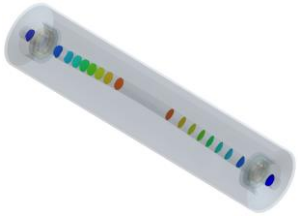	**3** 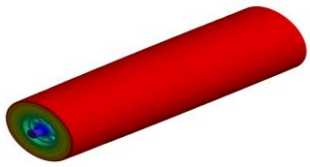
4 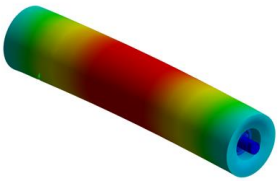	**5** 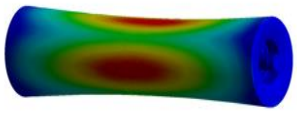	**6** 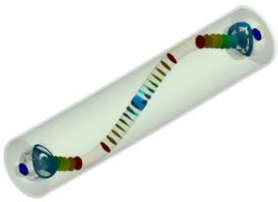
7 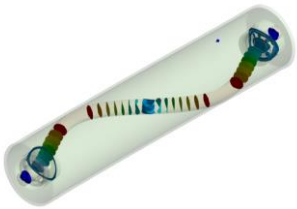	**8** 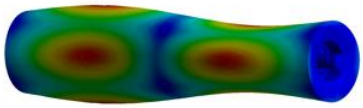	**9** 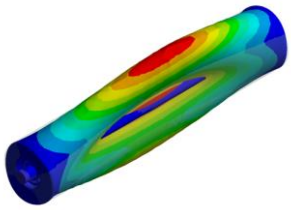
10 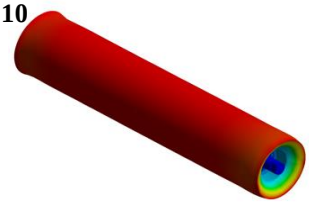		

A.2 Product design phase: Function and mean tree (Conveyor Idler)

In the rational method of product design, the Function and Mean Tree is established to set the functional requirements of the roller. Moreover, once these functions are identified, the specification tree mentioned in the report is then developed to outline the detailed specifications necessary to fulfil those functions effectively. Additionally, for other specifications of conveyor system technical drawing of LKAB TR010 Narvik Facility [32] will be also presented below.

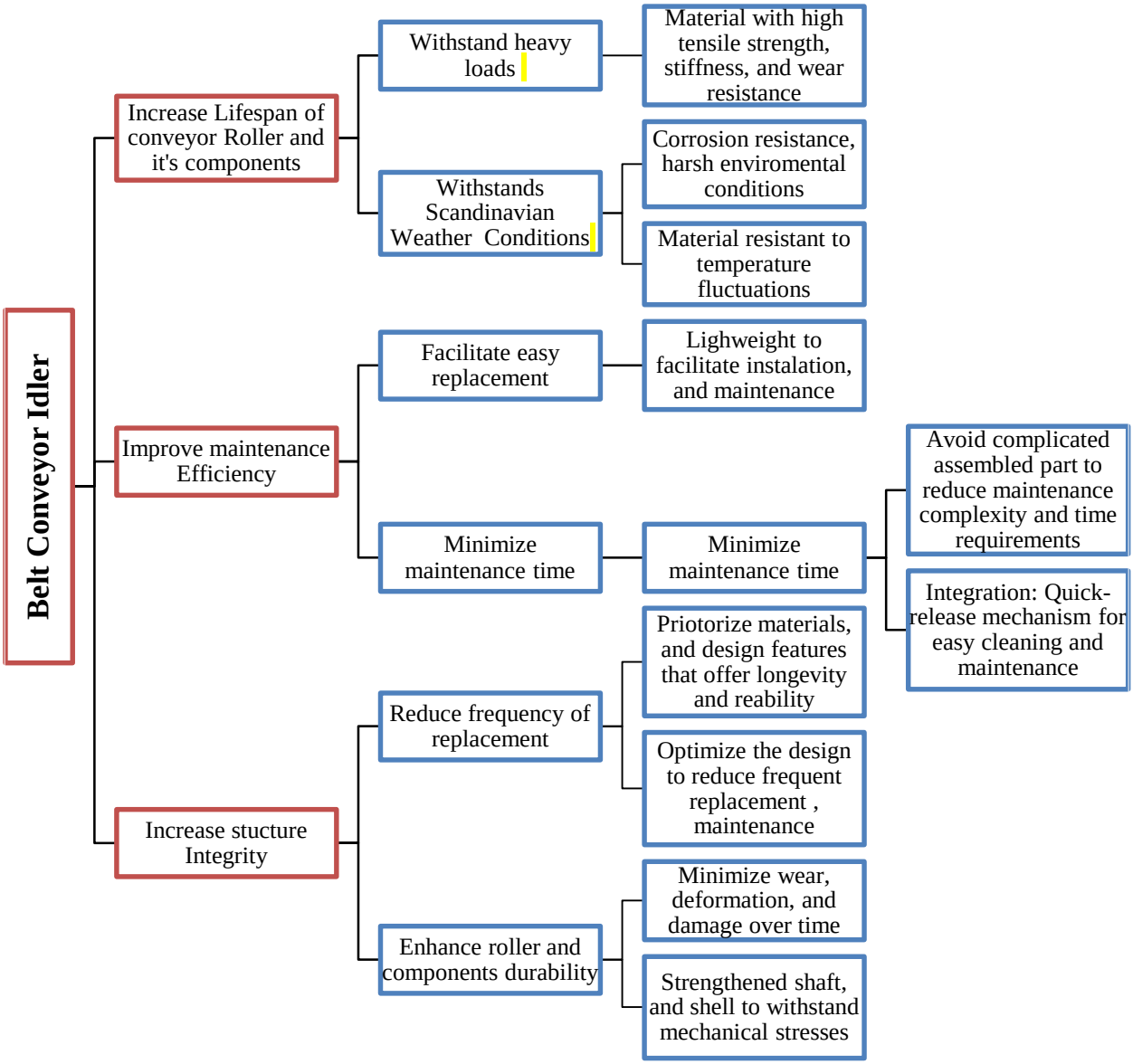

Denna ritning är LKAB:s egendom och får icke delgivas tredje man, kopieras, mångfaldigas eller på annat sätt utnyttjas utan bolagets medgivande.

LUOSSAVAARA-KIIRUNAVAARA AKTIEBOLAG

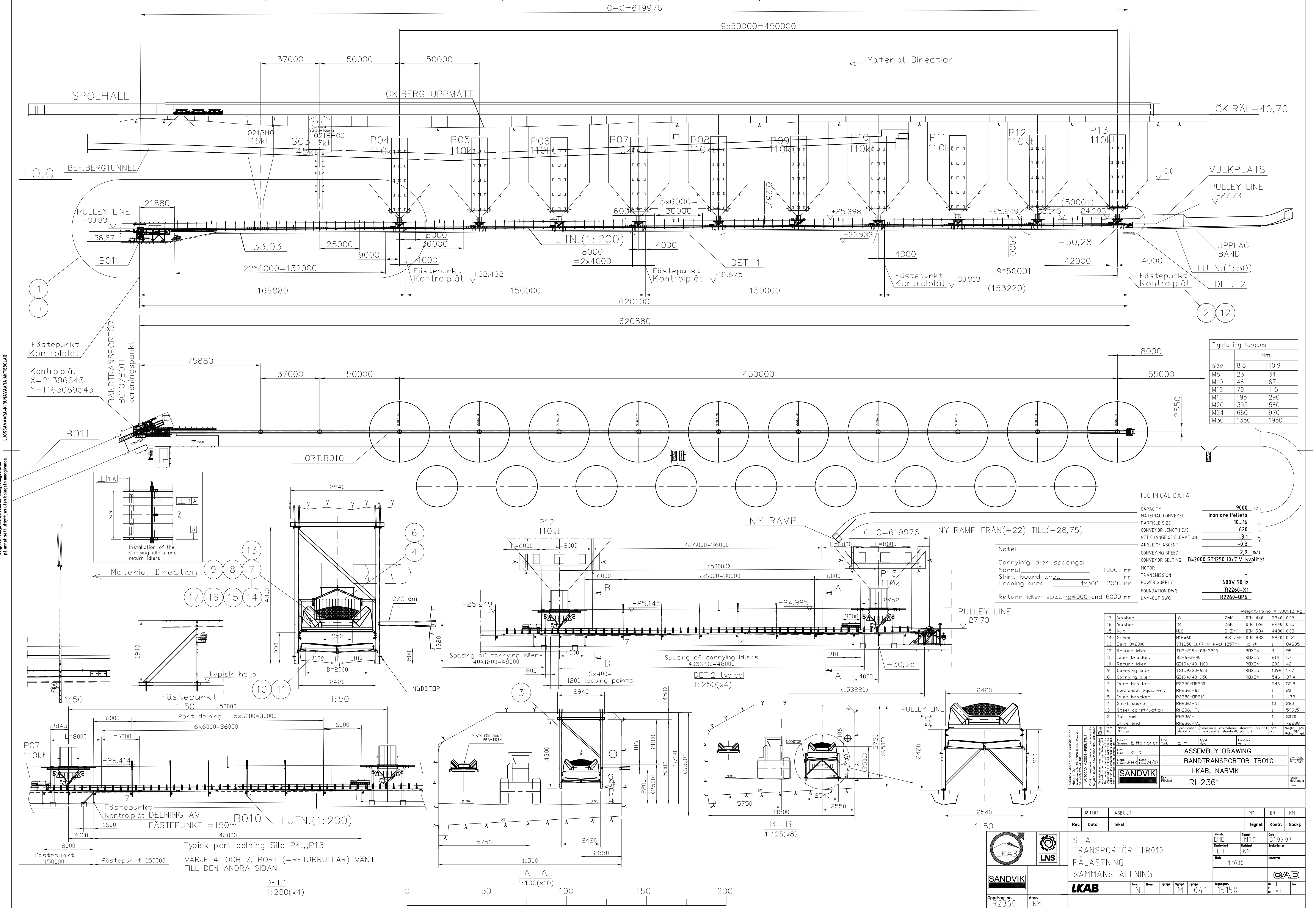

Note!
Carrying idler spacings:
Normal 1200 mm
Skirt board area mm
Loading area 4x300=1200 mm
Return idler spacing 4000 and 6000 mm

TECHNICAL DATA

CAPACITY	9000	t/h
MATERIAL CONVEYED	Iron ore Pellets	
PARTICLE SIZE	10...16	mm
CONVEYOR LENGTH C/C	620	m
NET CHANGE OF ELEVATION	-3,1	m
ANGLE OF ASCENT	-0,3	°
CONVEYING SPEED	2,9	m/s
CONVEYOR BELTING	B=2000 ST1250 10+7 V-kvalitet	
MOTOR	-	
TRANSMISSION	-	
POWER SUPPLY	400V 50Hz	
FOUNDATION DWG	R2260-X1	
LAY-OUT DWG	R2260-OP6	

Tightening torques

size	8.8 (Nm)	10.9 (Nm)
M8	23	34
M10	46	67
M12	79	115
M16	195	290
M20	395	560
M24	680	970
M30	1350	1950

Weight/Paino = 308912 kg

Item Osa	Name Nimitys	Specification (dimensions, rawmaterial, standard, drw.nr.) Merkki (mitat, raaka-aine, standardi, piir.no.)			pcs kpl	Weight Paino kg/pcs kpl
17	Washer	18	ZnK	DIN 440	2240	0.05
16	Washer	18	ZnK	DIN 126	2240	0.05
15	Nut	M16	8 ZnK	DIN 934	4480	0.03
14	Screw	M16x60	8.8 ZnK	DIN 933	2240	0.12
13	Belt B=2000	ST1250 10+7 V-kval 1257m+		joint	1	84395
12	Return idler	TH2-219-40B-2200		ROXON	4	98
11	Idler bracket	BDH6-3-40		ROXON	214	1.7
10	Return idler	GB194/40-1100		ROXON	206	42
9	Carrying idler	TS159/30-600		ROXON	1092	17.7
8	Carrying idler	GB194/40-950		ROXON	546	37.4
7	Idler bracket	R2350-OP200			546	55.8
6	Electrical equipment	RH2361-B1			1	20
5	Idler bracket	R2350-OP210			1	1173
4	Skirt board	RH2361-N1			10	280
3	Steel construction	RH2361-T1			1	59915
2	Tail end	RH2361-L1			1	8070
1	Drive end	RH2361-V1			1	72288

Sandvik Mining and Construction Hollola Oy
Keskikankaantie 19, 15860 Hollola, Finland
Tel: +358 205 44 181

AUTOCAD V.2004-PIIRUSTUS
Kaikki muutokset ilmoitettava suunnittelijalle kuvan päivittämiseksi arkistoon

Design Suunn. E.Heinonen | Chd. Tark. E.H | Appd. Hyv. | Cust.no. As.no.

Dept. Osasto EHK | Date Pvm 24/07

ASSEMBLY DRAWING
BANDTRANSPORTÖR TR010
LKAB, NARVIK

SANDVIK

Drw.nr. Piir.N:o RH2361 | Issue Muutostila —

Rev.	Dato	Tekst	Tegnet	Kontr.	Godkj.
	18.11.09	ASBUILT	MP	EH	KM

SILA
TRANSPORTÖR_TR010
PÅLASTNING
SAMMANSTÄLLNING

Konstr. EHE | Tegnet MTO | Dato 31.06.07
Kontrollert EH | Godkjent KM
Skala 1:1000

LKAB | N | M | 041 | 15150 | Bl. 1 | Rev. -
A1

SANDVIK LKAB LNS CAD

Oppdrag nr. R2360 | Ansv. KM

Appendix B: Supplementary Study

a) Analytical Calculation For Wing Idler:

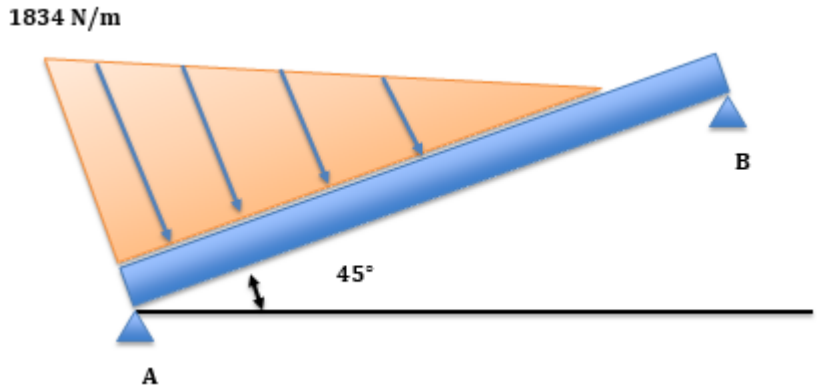

Figure B–1: Wing Roller position

First we start by drawing the free body diagram of the roller; and replacing each of the support by its equivalent components, similarly for the triangular distributed load and rollers own weight.

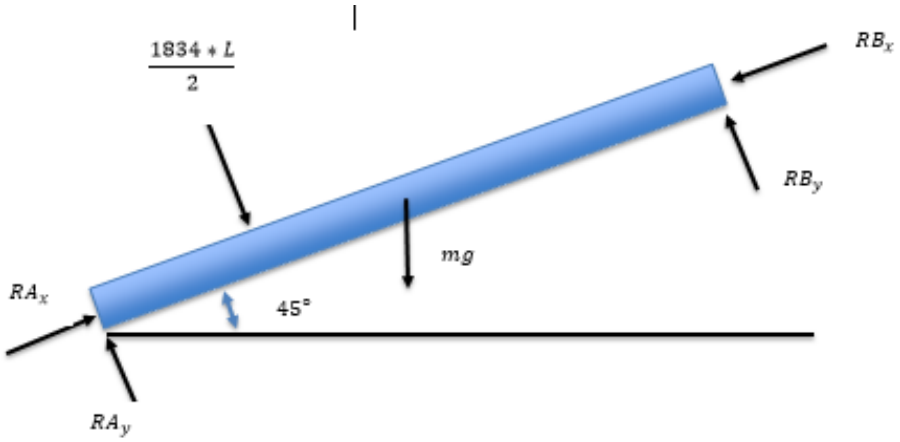

Figure B–2: Wing Roller Free body diagram

Where; RA, RB are the components of the pin supports at points A, B respectively, mg represent the rollers weight acting at the middle of the roller positioned vertically downward. Moreover, the distributed load is replaced by its resultant force placed at a distance one third from the biggest side.

Now solving the equilibrium equations:

$$\sum F_x = 0 \qquad (1)$$

$$\sum F_x = RA_x - RB_x - mg\cos(45) = 0$$

$$\sum F_y = 0 \tag{2}$$

$$\sum F_y = RA_y + RB_y - mg\sin(45) - \left(550 \times \frac{L}{2}\right) = 0$$

$$\sum M_A = 0 \tag{3}$$

$$\sum M_A = (RB_y L) - mg\sin(45) * \left(\frac{L}{2}\right) - \left(550 \times \frac{L}{2}\right) \times \frac{L}{3} = 0$$

Solving Equilibrium equations reveals:

$RB_y = 100N, RA_y = 150N$

But, still the x-components of the supports at A, B are unknown due to the fact that the above system is a statically indeterminate system, where the number of unknowns is greater than the number of equilibrium equations.

Therefore, to solve such a system, compatibility equation is needed. Since the supports are excreting forces in x-direction, preventing the displacement of the roller in that direction.
Then using the equation of total displacement in roller equals to zero:

$$\Delta_{total} = \Delta_{BD} + \Delta_{DC} = 0 \tag{4}$$

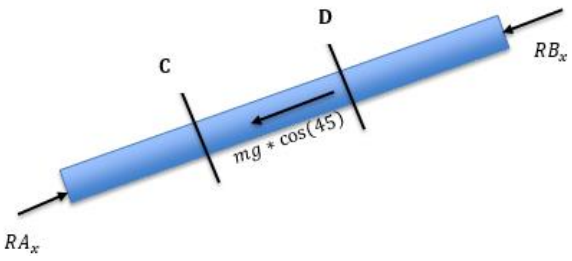

Figure B–3: Wing roller free body diagram

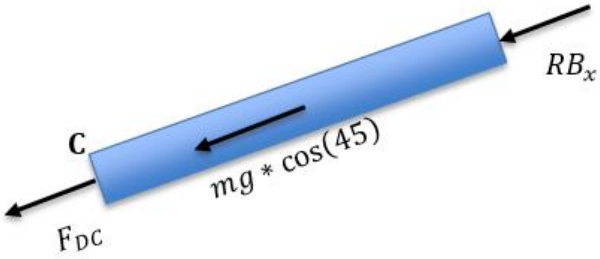

Therefore, the 4th equation (compatibility equation) will be as follows: Now applying a cut at section D, C respectively,

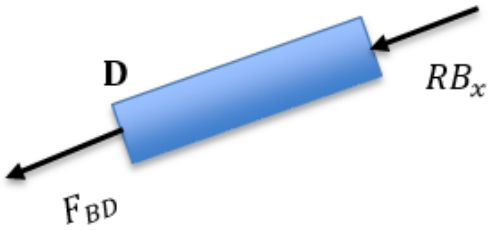

Figure B–4: Wing Roller cuts section C, D respectively

From section D, C $\sum F_x = 0$ respectively:

Section D:

$$-RB_x = F_{DB}$$

Section C:

$$-F_{DC} - RB_x - mg\cos(45) = 0$$

$$F_{DC} = -(RB_x + mg\cos(45)) = 0$$

But as stated before total deformation of the roller is zero. Therefore:

$$\Delta_{total} = \Delta_{BD} + \Delta_{DC} = 0$$

Thus,

$$\Delta_{BD} = \frac{-RB_x L}{AE} = \frac{-RB_x \frac{L}{2}}{AE}$$

$$\Delta_{DC} = \frac{-(RB_x + mg\cos(45)) * \frac{L}{2}}{AE}$$

A : Cross-section area of roller, E modulus of elasticity.

Inserting Δ_{BD}, Δ_{DC} into 4 and solving for RB_x reveals:

$RB_x = -54N$; substituting in (1) thus $RA_x = 53N$

Wing Idler APDL Analysis Results:

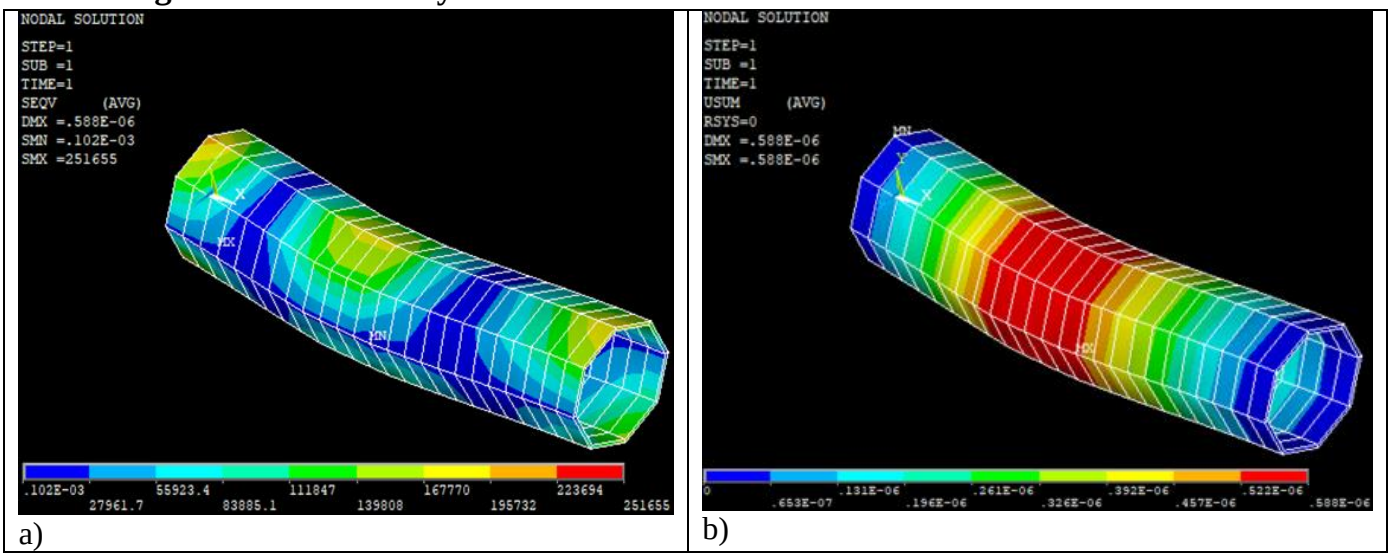

a) b)

Figure B–5: Wing roller shell a) Von-misses Stress (Pa), b) Deflection (m)

Beam Deflection Equation Integration Method:

Another way to calculate the maximum deflection in a beam other that using the formulas directly is to derivate the beam deflection curve. For the studied case, it is assumed to be fixed supported at both ends the after applying the integration of equation. Integrating the following equation we get shear force:

$$EI \times \left(\frac{d^2y}{dx^2}\right) = M \tag{38}$$

$$EI \times \left(\frac{d^3y}{dx^3}\right) = (F_{center\_distributed})\, x + A\,, \tag{39}$$

Integrating (39) to get moment equation:

$$EI \times \left(\frac{d^2y}{dx^2}\right) = (F_{center\_distributed})\frac{x^2}{2} + Ax + B\,, \tag{40}$$

Integrating (40) to get the slope equation:

$$EI \times \left(\frac{dy}{dx}\right) = (F_{center\_distributed})\frac{x^3}{6} + \frac{Ax^2}{2} + Bx + C\,, \tag{41}$$

Finally, integrating (41) to get the deflection equation:

$$EIy = (F_{center\_distributed})\,\frac{x^4}{24} + \frac{Ax^3}{6} + \frac{Bx^2}{2} + Cx + D\,, \tag{42}$$

Now applying the boundary conditions of fixed ends, and calculate the integration constants.

b) Bearing study Summary

Theoretical lifespan of bearings Rolling contact fatigue (RCF) estimation is based on factors such as load, speed, lubrication, and material properties. However, in practical applications, bearings may fail before reaching their calculated fatigue life due to various reasons.

Table B-1: Factors influencing bearing performance and lifespan in conveyor systems

Factors	**Description**
Operating Conditions	Higher loads, elevated temperatures, inadequate lubrication, or contamination that may accelerate fatigue damage and lead to premature failure.
Dynamic Load Variations	Rapid changes in load or speed, as well as shock loads or vibrations, can increase stress concentrations in the bearing and shorten its lifespan.
Material Defects	Inherent material defects or manufacturing irregularities in bearings can reduce their fatigue strength and compromise their reliability, can lead to premature failure, particularly under high-stress conditions.
Environmental Factors	Harsh operating environments, exposure to contaminants, or corrosive substances can degrade bearing materials and lubricants, leading to accelerated wear and fatigue. Environmental factors that are not accounted for in RCF calculations can significantly impact bearing performance and lifespan.

As a conclusion bearings may fail before reaching their calculated fatigue life. Therefore, while RCF calculations provide valuable insights into bearing performance and reliability, it's essential to consider real-world operating conditions and potential failure modes when assessing bearing lifespan and implementing maintenance strategies. Regular monitoring, proper maintenance practices, and selecting bearings with sufficient margin can help mitigate the risk of premature failure and ensure reliable operation in practical applications.

Ansys GRANTA EDUPACK

Stage 1: Young's modulus (GPa) vs. Density (kg/m^3)

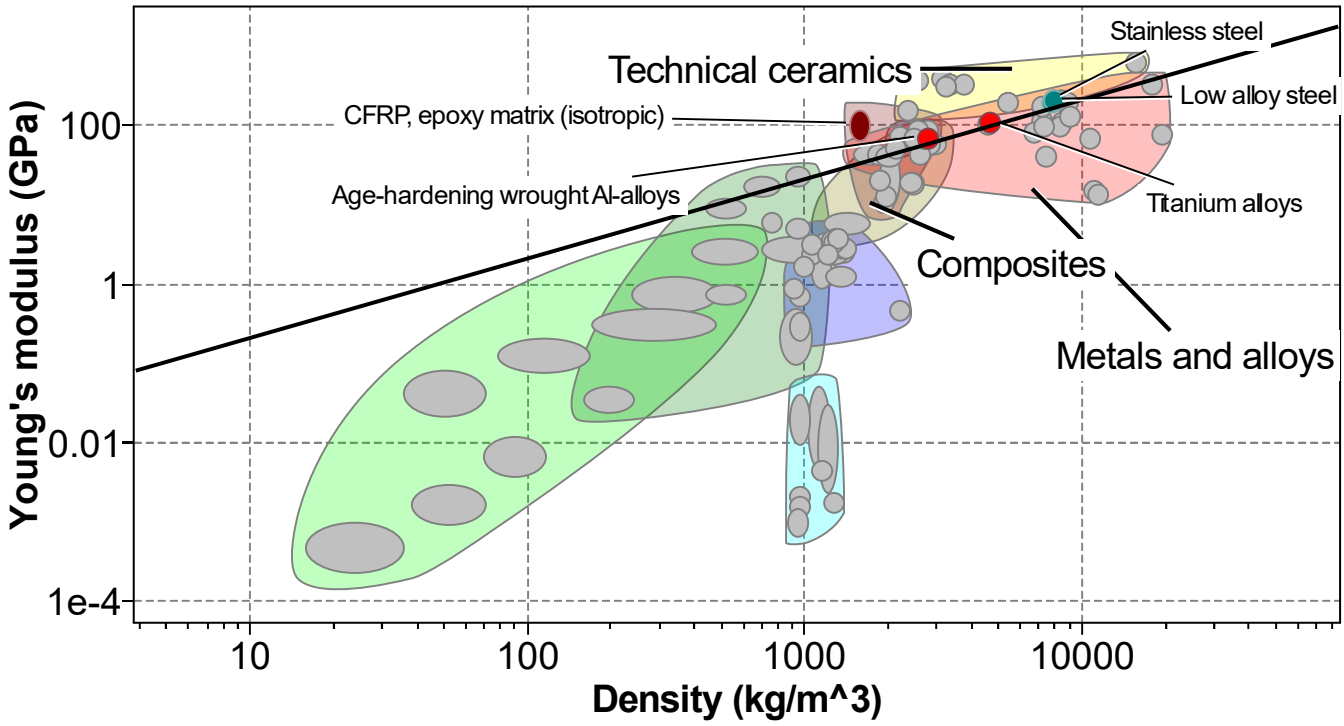

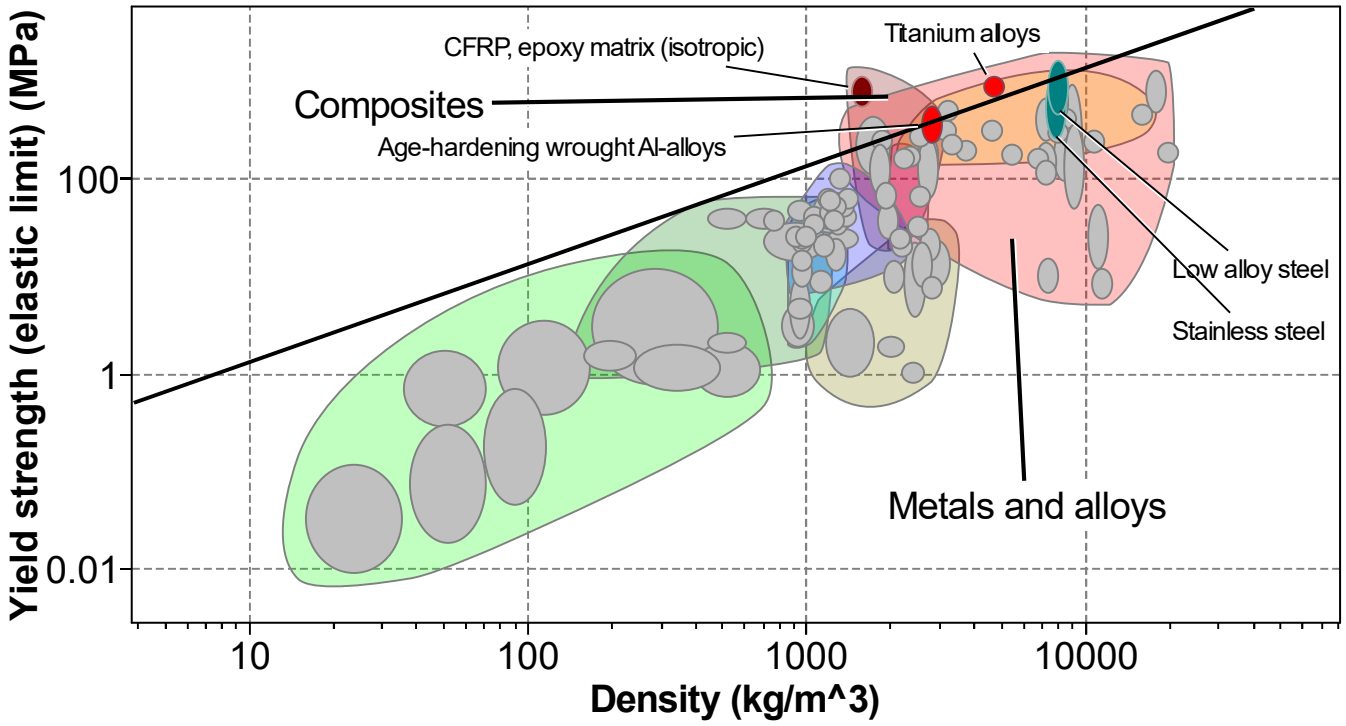

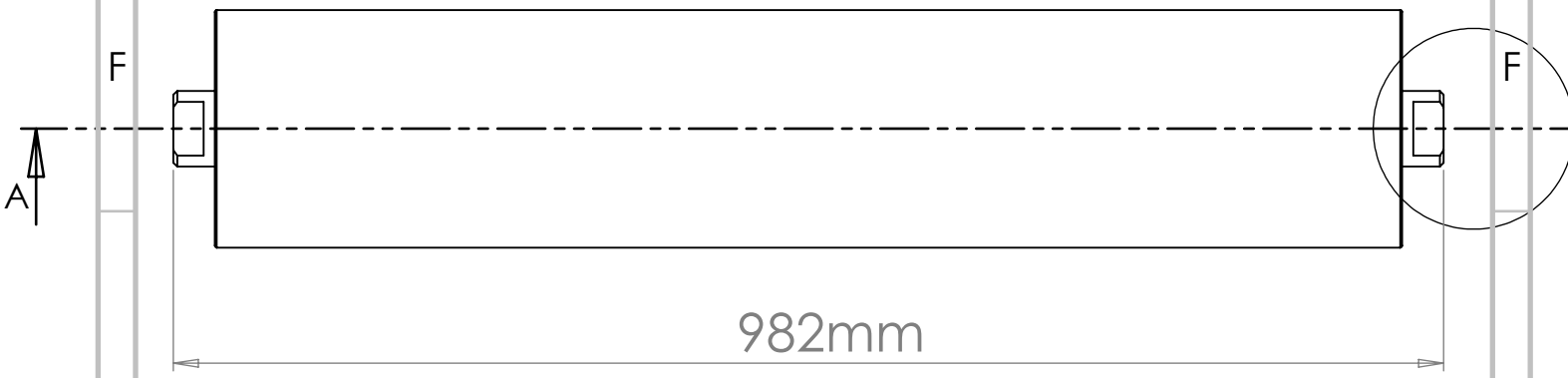

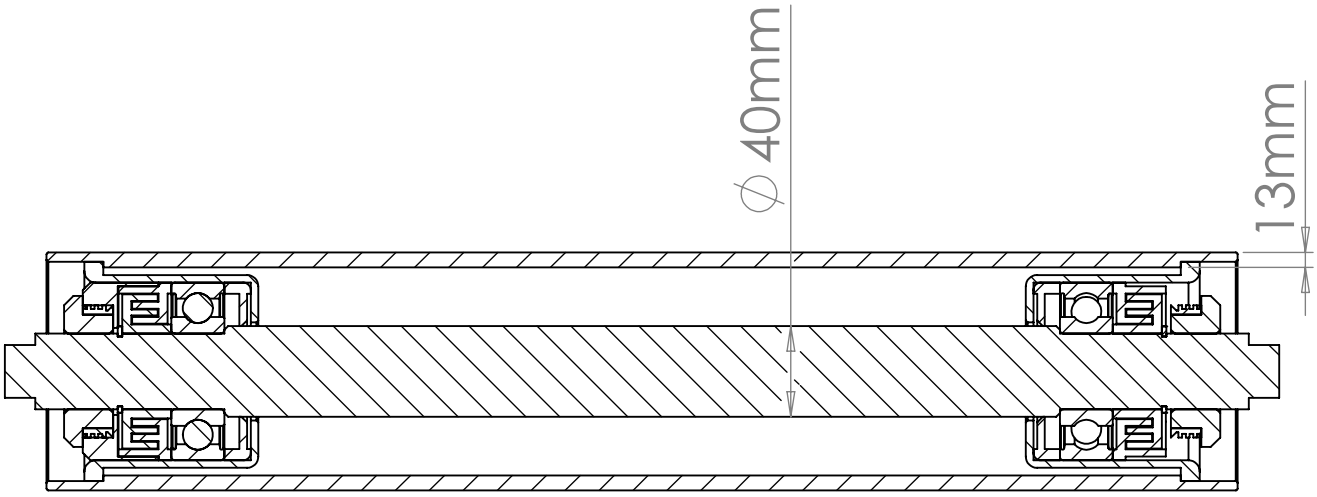

SECTION A-A
SCALE 1 : 2

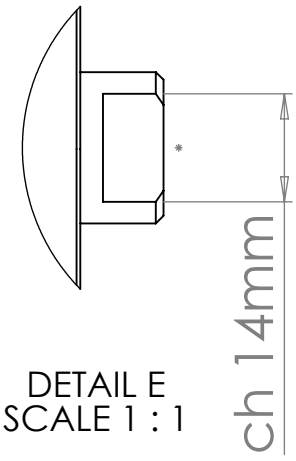

DETAIL E
SCALE 1 : 1

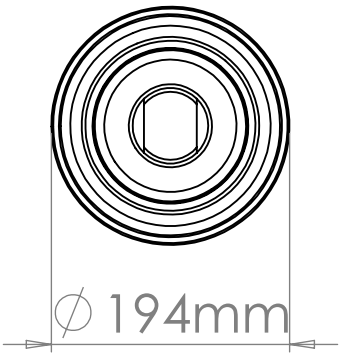

UNLESS OTHERWISE SPECIFIED: DIMENSIONS ARE IN MILLIMETERS SURFACE FINISH: TOLERANCES: LINEAR: ANGULAR:	FINISH:		DEBURR AND BREAK SHARP EDGES	DO NOT SCALE DRAWING	REVISION		
	NAME	SIGNATURE	DATE	TITLE:			
DRAWN	Ahmad Fadel		17-April-24	Roller Assembly Dimensions			
CHK'D							
APPV'D							
MFG							
Q.A				MATERIAL: 1-Roller Shell (HDPE) 2-Roller Shaft (Stainless-steel)	DWG NO. DWG-001	A4	
				WEIGHT:	SCALE:1:5	SHEET 1 OF 2	

ITEM NO.	PART NAME	QTY.
1	Roller Shell	1
2	Shaft	1
3	External Cover	2
4	Washer	2
5	Bearing Housing	2
6	Circlip	2
7	Labyrinth Seal	4
8	6308 SKF Deep Groove Ball Bearing	2
9	Internal Seal	2

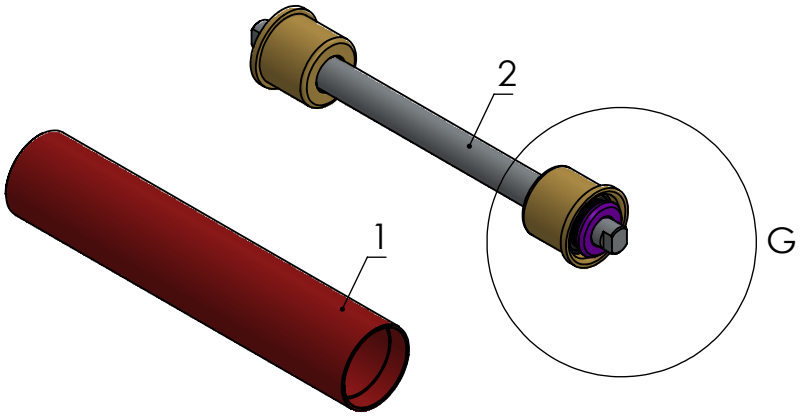

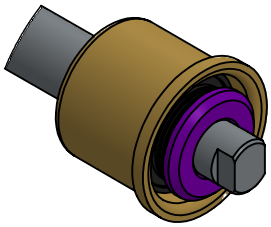

DETAIL G
SCALE 2 : 5

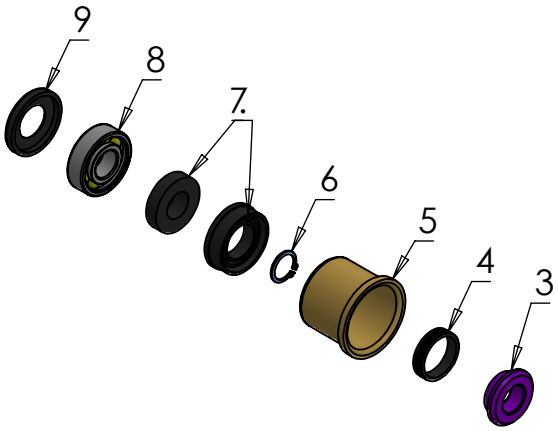

UNLESS OTHERWISE SPECIFIED: DIMENSIONS ARE IN MILLIMETERS SURFACE FINISH: TOLERANCES: LINEAR: ANGULAR:		FINISH:		DEBURR AND BREAK SHARP EDGES	DO NOT SCALE DRAWING	REVISION	
	NAME	SIGNATURE	DATE		TITLE:		
DRAWN	Ahmad Fadel		17- April-24		**Bearing Assembly Detail**		
CHK'D							
APPV'D							
MFG							
Q.A				MATERIAL:	DWG NO.		A4
					DWG-002		
				WEIGHT:	SCALE:1:5	SHEET 2 OF 2	

diagram 2 - Estimation of the rated viscosity v_1

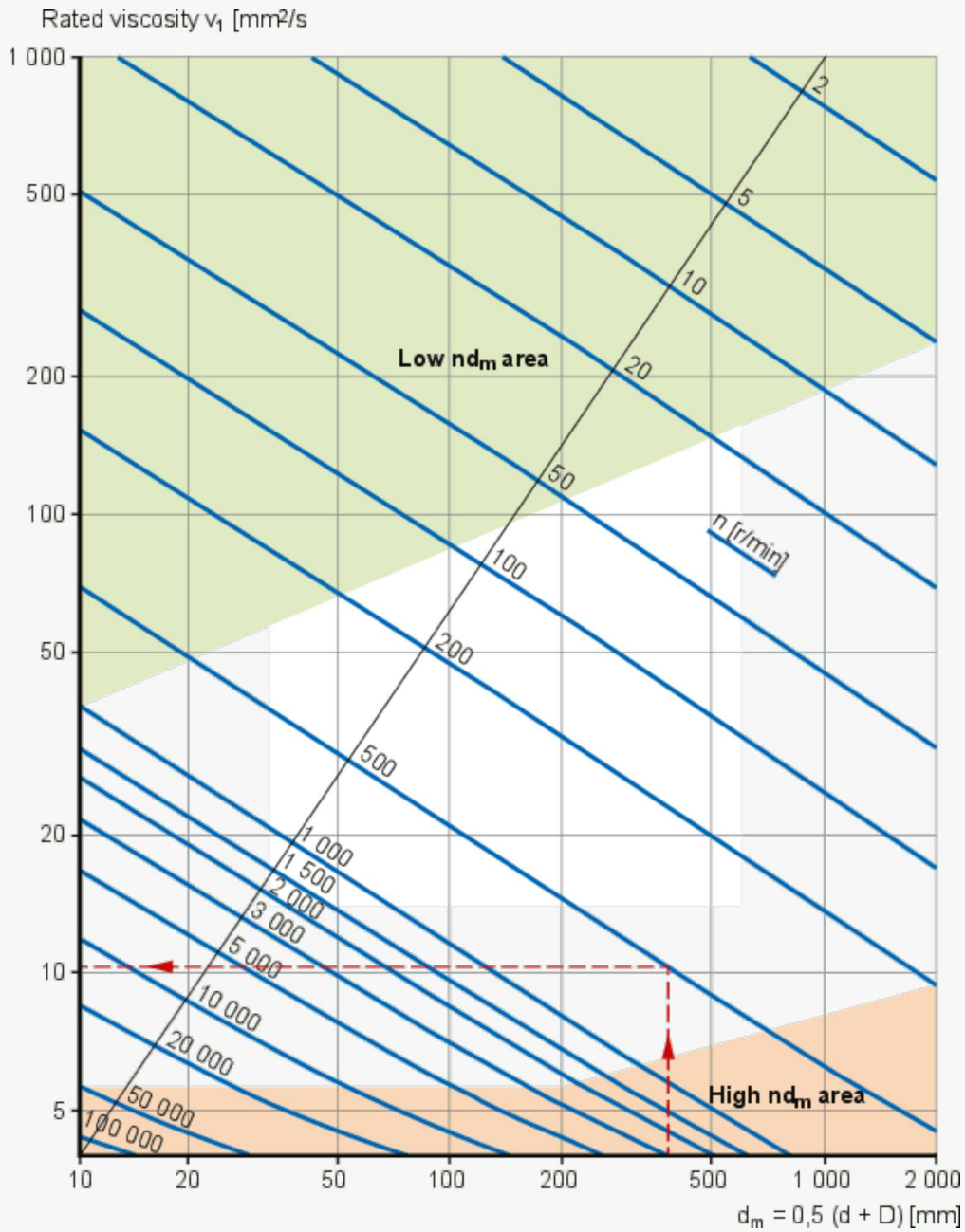

Green shading shows the area where $nd_m \leq 10{,}000$ [mm/min]. At these lower nd_m values, AW or EP additives are needed to reduce wear.

Orange shading shows the area where $nd_m \geq 500{,}000$ [mm/min] for up to 200 mm bearing mean diameter, and $nd_m \geq 400{,}000$ [mm/min] for larger bearing mean diameters. At these higher nd_m values, operating temperature must be given more attention. Certain bearing types, such as spherical roller bearings, tapered roller bearings and spherical roller thrust bearings, normally have a higher operating temperature than others, such as deep groove ball bearings and cylindrical roller bearings, under comparable operating conditions.

diagram 2 - Estimation of the rated viscosity v_1

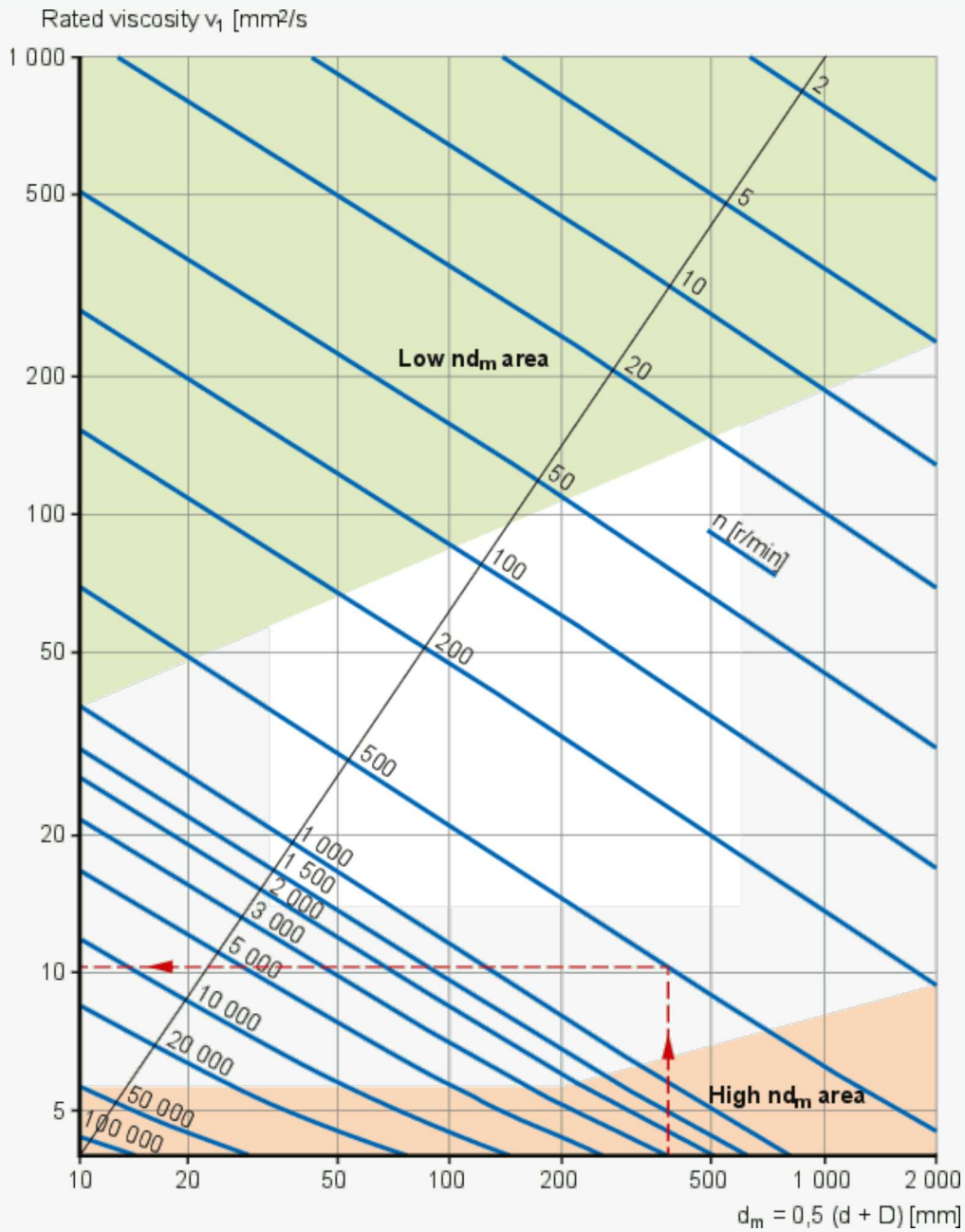

Green shading shows the area where $nd_m \leq 10{,}000$ [mm/min]. At these lower nd_m values, AW or EP additives are needed to reduce wear.

Orange shading shows the area where $nd_m \geq 500{,}000$ [mm/min] for up to 200 mm bearing mean diameter, and $nd_m \geq 400{,}000$ [mm/min] for larger bearing mean diameters. At these higher nd_m values, operating temperature must be given more attention. Certain bearing types, such as spherical roller bearings, tapered roller bearings and spherical roller thrust bearings, normally have a higher operating temperature than others, such as deep groove ball bearings and cylindrical roller bearings, under comparable operating conditions.

diagram 1 - Viscosity-temperature diagram for ISO viscosity grades (Mineral oils, viscosity index 95)

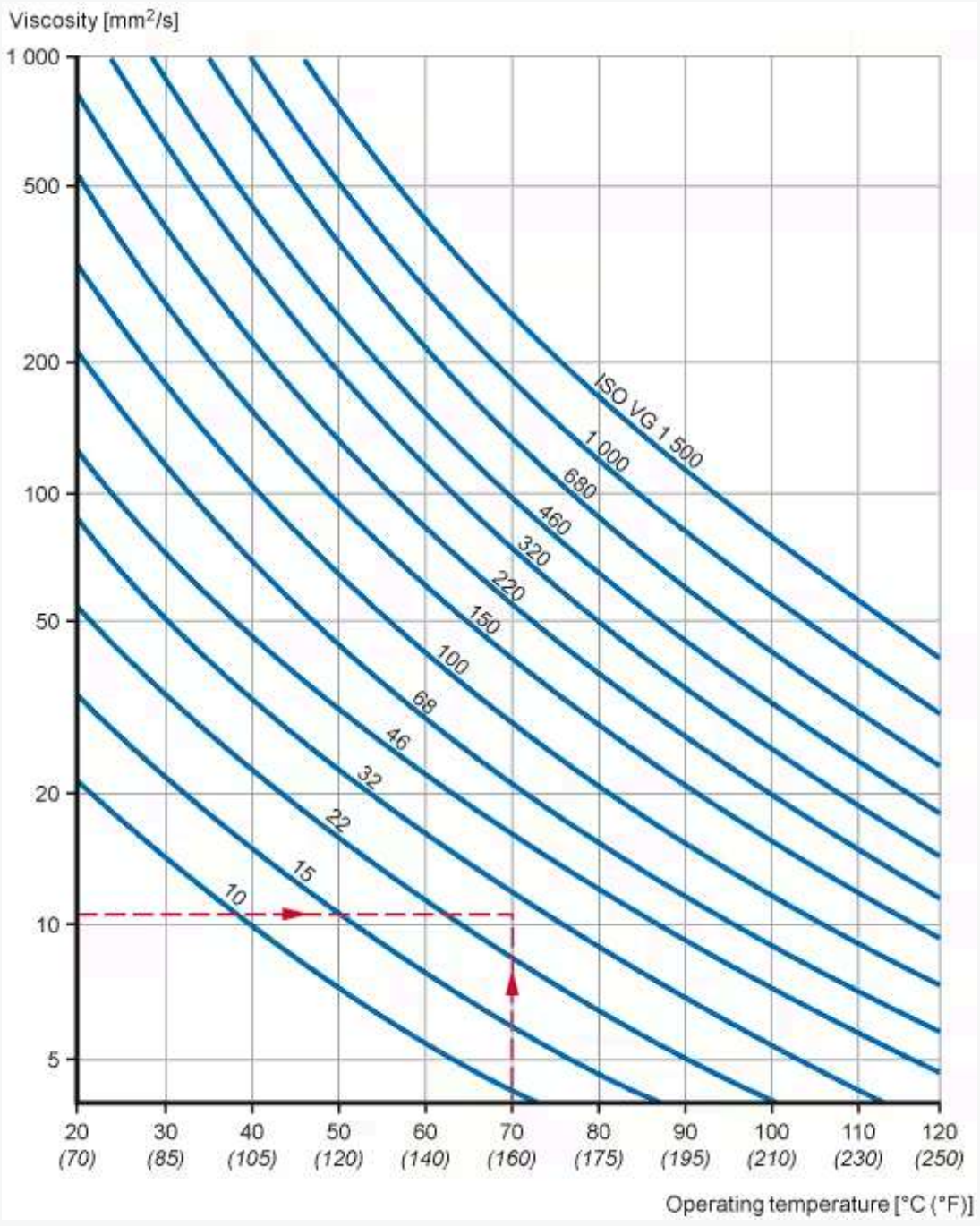

diagram 2 - Relubrication intervals at operating temperatures of 70 °C (160 °F)

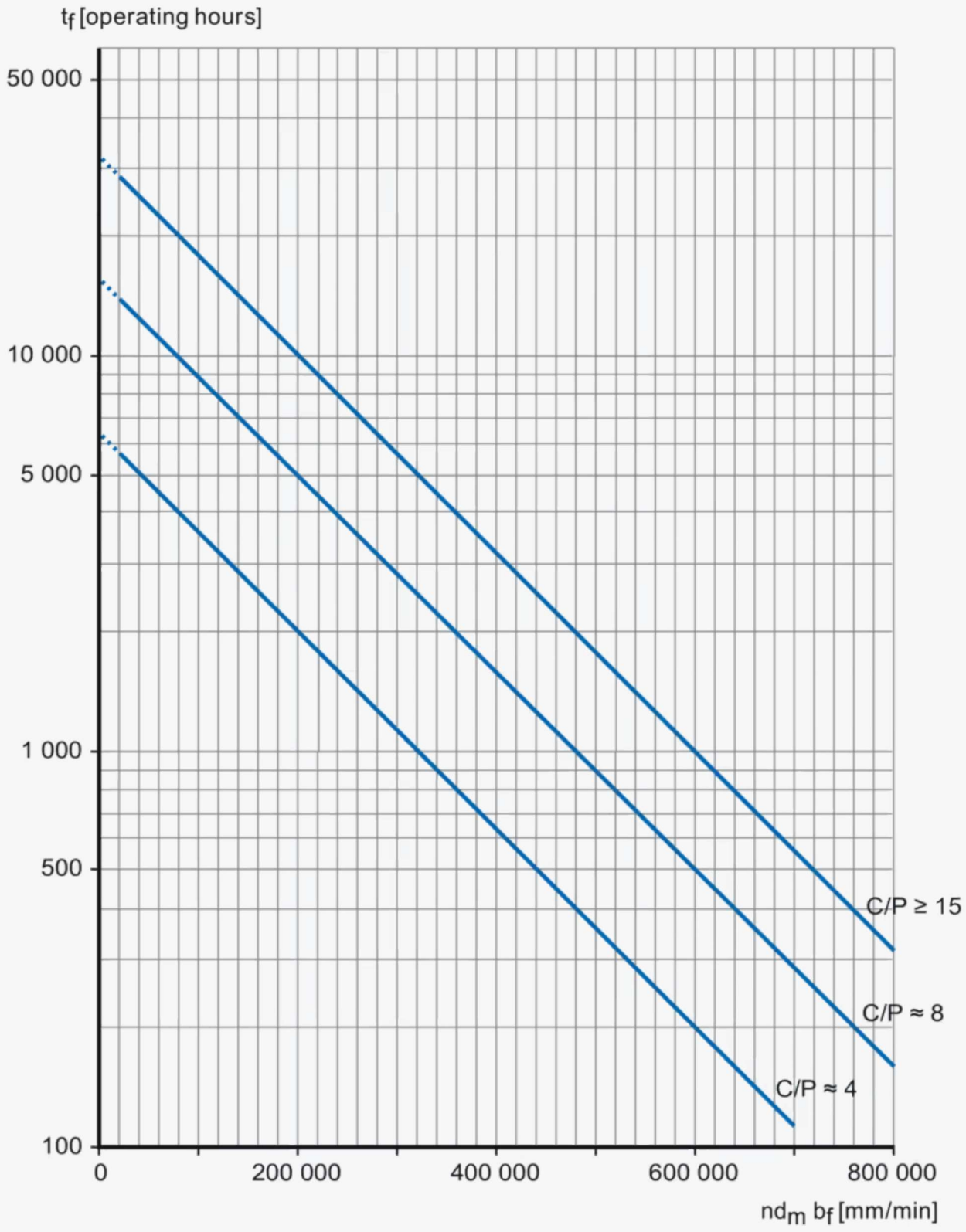

table 1 - Bearing factors and recommended nd_m limits

Bearing type[1]	Bearing factor	Recommended nd_m limits for load ratio		
	b_f	C/P ≥ 15	C/P ≈ 8	C/P ≈ 4
–	–	mm/min		
Deep groove ball bearings	1	500 000	400 000	300 000
Angular contact ball bearings	1	500 000	400 000	300 000
Self-aligning ball bearings	1	500 000	400 000	300 000
Cylindrical roller bearings				
– non-locating bearing	1,5	450 000	300 000	150 000
– locating bearing, without external axial loads				
... or with light but alternating axial loads	2	300 000	200 000	100 000
– locating bearing, with constantly acting light axial load	4	200 000	120 000	60 000
– without a cage, full complement[2]	4	NA[3]	NA[3]	20 000
Needle roller bearings				
– with a cage	3	350 000	200 000	100 000
Tapered roller bearings	2	350 000	300 000	200 000
Spherical roller bearings				
– when the load ratio $F_a/F_r \leq e$ and $d_m \leq 800$ mm				
... series 213, 222, 238, 239	2	350 000	200 000	100 000

series 223, 230, 231, 232, 240, 248, 249	2	250 000	150 000	80 000
series 241	2	150 000	80 000	50 000
– when the load ratio $F_a/F_r \leq e$ and $d_m > 800$ mm				
series 238, 239	2	230 000	130 000	65 000
series 230, 231, 232, 240, 248, 249	2	170 000	100 000	50 000
series 241	2	100 000	50 000	30 000
– when the load ratio $F_a/F_r > e$				
all series	6	150 000	50 000	30 000
CARB toroidal roller bearings				
– with a cage	2	350 000	200 000	100 000
– without a cage, full complement[2)]	4	NA[3)]	NA[3)]	20 000
Thrust ball bearings	2	200 000	150 000	100 000
Cylindrical roller thrust bearings	10	100 000	60 000	30 000
Needle roller thrust bearings	10	100 000	60 000	30 000
Spherical roller thrust bearings				
– rotating shaft washer	4	200 000	120 000	60 000

[1)]The bearing factors and recommended nd_m limits apply to bearings with standard internal geometry and standard cage execution. For alternative internal bearing design and special cage execution, contact the SKF application engineering service.
[2)]The t_f value obtained from diagram a needs to be divided by a factor of 10.
[3)]Not applicable, as a bearing with a cage is recommended for these C/P values.

Table 1 - Viscosity classification to ISO 3448

Viscosity grade	Kinematic viscosity limits at 40 °C *(105 °F)*		
	mean	min.	max.
-	mm^2/s		
ISO VG 2	2,2	1,98	2,42
ISO VG 3	3,2	2,88	3,52
ISO VG 5	4,6	4,14	5,06
ISO VG 7	6,8	6,12	7,48
ISO VG 10	10	9,00	11,0
ISO VG 15	15	13,5	16,5
ISO VG 22	22	19,8	24,2
ISO VG 32	32	28,8	35,2
ISO VG 46	46	41,4	50,6
ISO VG 68	68	61,2	74,8
ISO VG 100	100	90,0	110
ISO VG 150	150	135	165
ISO VG 220	220	198	242
ISO VG 320	320	288	352
ISO VG 460	460	414	506
ISO VG 680	680	612	748
ISO VG 1 000	1 000	900	1 100
ISO VG 1 500	1 500	1 350	1 650

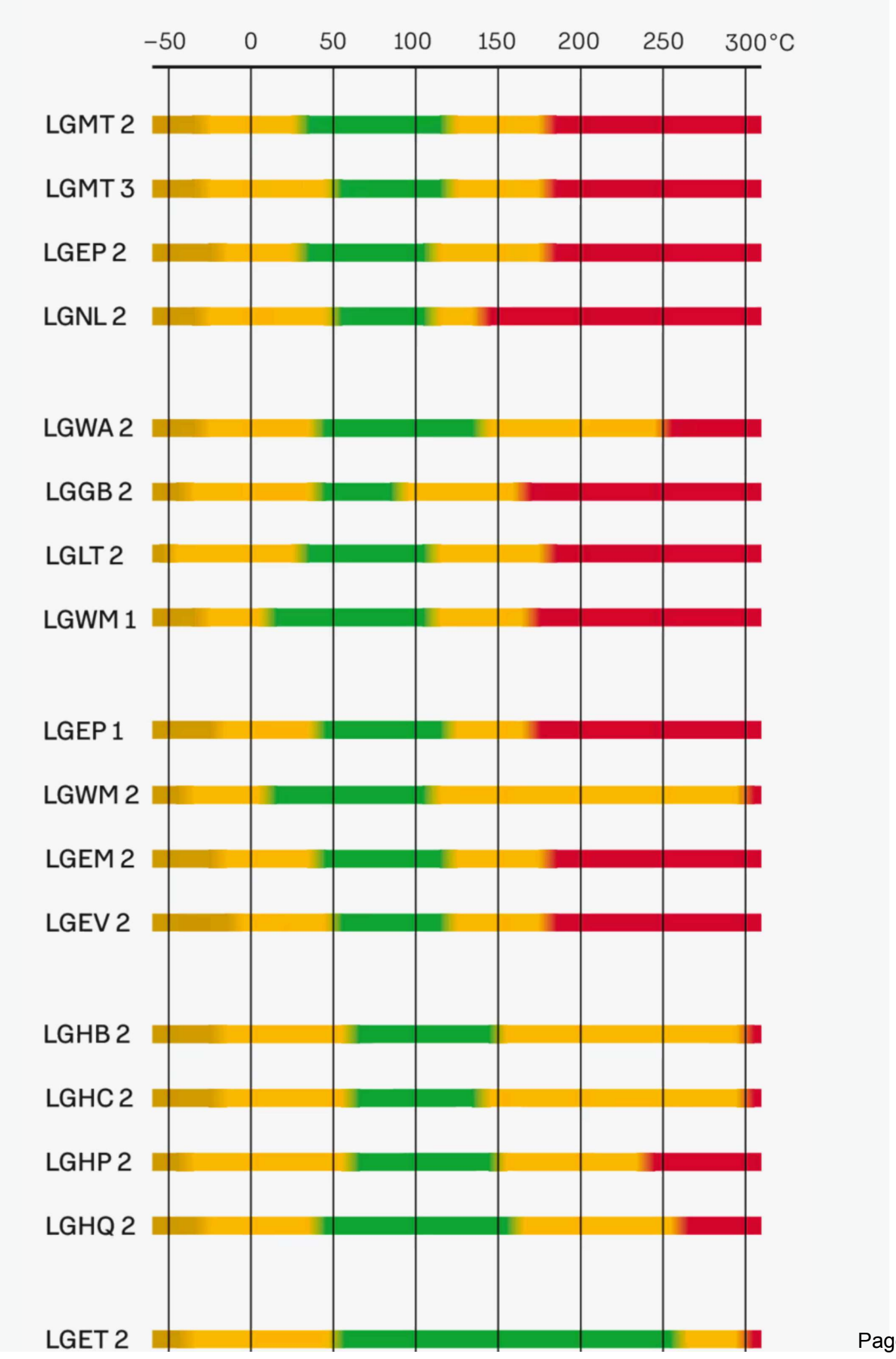
−50
0
50
100
150
200
250
300 °C
LGMT 2
LGMT 3
LGEP 2
LGNL 2
LGWA 2
LGGB 2
LGLT 2
LGWM 1
LGEP 1
LGWM 2
LGEM 2
LGEV 2
LGHB 2
LGHC 2
LGHP 2
LGHQ 2
LGET 2

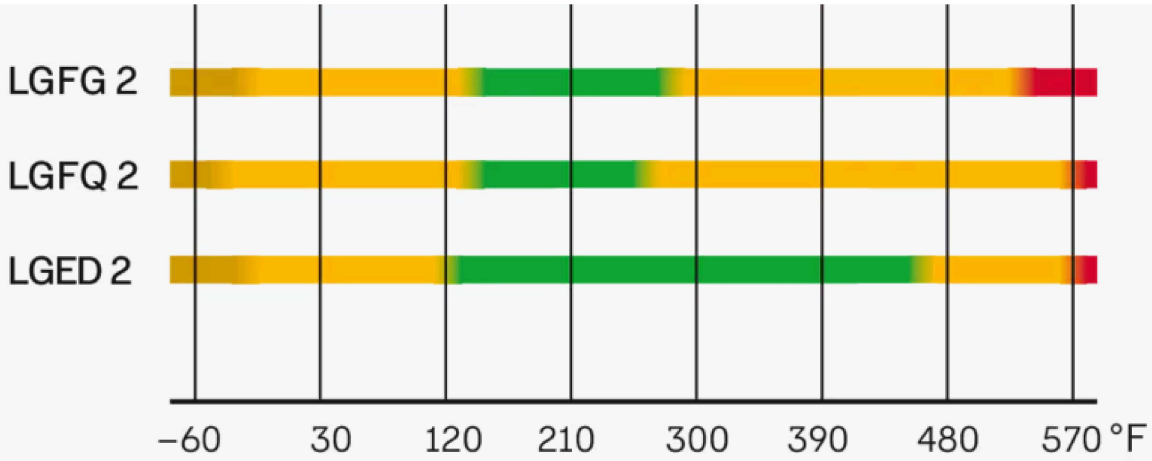

[1)]The low temperature performance limits (LTPL) are valid for roller bearings. LTPL values for ball bearings are approx. 20 °C *(35 °F)* lower.